Sphingolipid depletion inhibits bulk endocytosis while triggering selective clearance of the methionine transporter Mup1

Nathaniel L. Hepowit[1], Bradley Moon[1], Robert C. Dickson[2] *, and Jason A. MacGurn[1] *

[1] Department of Cell and Developmental Biology, Vanderbilt University, Nashville, United States

[2] Department of Molecular and Cellular Biochemistry, University of Kentucky, Lexington, United States

* For correspondence: bobd@uky.edu; jason.a.macgurn@vanderbilt.edu

Abstract

Myriocin is a potent inhibitor of sphingolipid biosynthesis that increases lifespan in a variety of model organisms, but how slowing sphingolipid biosynthesis promotes longevity remains unknown. Previously, we reported that myriocin treatment of yeast cells triggers an acute decline in the abundance of most amino acids, resulting in a state of amino acid restriction. Myriocin also triggers the endocytic downregulation of the methionine transporter Mup1, although its effect on other nutrient transporters is unknown. Here, we characterized a panel of different PM proteins – including amino acid transporters, hexose transporters, proton pumps, and signaling receptors – during a myriocin treatment time course. In contrast to Mup1, all other PM proteins examined were either unaffected or accumulated at the PM in response to myriocin treatment. Notably, myriocin treatment inhibits bulk endocytosis after 4 hours of treatment, which may account for the accumulation of various PM proteins in response to myriocin. Our data indicates that the mechanism of myriocin-induced Mup1 endocytosis is distinct from methionine-induced Mup1 endocytosis in that it is dependent on the Rsp5 adaptor Art2, C-terminal lysine residues, and the formation of K63-linked ubiquitin polymers. These findings shed new light on how cells adapt to sphingolipid depletion and reveal a novel mechanism for endocytic clearance of Mup1.

Introduction

Sphingolipids (SLs) are a diverse class of lipids that serve as a structural component of eukaryotic membranes but also have important regulatory functions related to cell signaling. The first steps of SL biosynthesis occur in the ER and result in the production of ceramide, which is then transported to the Golgi complex for further modification into complex SLs. These complex SLs are then transported to different membranes throughout the cell where they serve a multitude of functions [1]. For example, sphingomyelin regulates sorting of specific secretory cargo in the trans-Golgi network of mammalian cells [2, 3]. In the PM of mammalian cells, sphingosine 1-phosphate is generated and can be secreted to act as a signaling molecule that mediates complex processes including vascular development and coordination of immune responses [4]. In yeast, sphingolipids at the PM regulate the activation of TORC2 [5]. Indeed, the variety of regulatory functions served by SLs is underscored by their important role in processes that range from memory and cognition [6] to the progression of cancer [7, 8].

Myriocin (Myr) is a potent inhibitor of serine palmitoyltransferase (SPT) which catalyzes the first step of SL biosynthesis and increases lifespan in a variety of model organisms [9]. There is a growing body of data showing that Myr treatment reduces the severity of age-related diseases in mice and rats, including atherosclerosis and cardiac impairment [10-13], factors for metabolic syndrome, obesity, diabetes and cancer [14-18], amyloid beta and tau hyperphosphorylation in Alzheimer's disease [19] and other neurodegenerative diseases [20, 21]. Despite its therapeutic potential, it remains unclear how dampening SL biosynthesis confers these health benefits to enhance longevity.

Perturbations that alter sphingolipid homeostasis have complex effects on cellular processes, and how myriocin slows aging and supports longevity is currently unclear. Using the yeast *Saccharomyces cerevisiae*, we have worked to understand how myriocin treatment and sphingolipid depletion lead to increased longevity. Recently, we reported that Myr-treated yeast cells experience a state of amino acid restriction, which is associated with decreased uptake of

55 amino acids from the media into the cell. We also reported that Myr triggered the endocytic
56 clearance of the high affinity methionine transporter Mup1, although the fate of other nutrient
57 transporters remains unclear. Here, we report on how Myr affects a broad panel of different PM
58 proteins – including amino acid transporters, hexose transporters, proton pumps, and signaling
59 receptors. Our analysis reveals that Myr triggers selective endocytic clearance of Mup1 while
60 inhibiting bulk endocytosis, leading to PM accumulation of many other nutrient transporters. We
61 also address the mechanism of Myr-mediated Mup1 endocytosis, which is mechanistically distinct
62 from methionine-induced Mup1 endocytosis. These studies are crucial to understanding how Myr
63 treatment leads to a state of amino acid restriction, and they provide new insights into how the
64 PM is remodeled in response to sphingolipid depletion.
65
66

67 **Results**

68 **Myriocin triggers remodeling of AAT composition at the PM**

69 Our previous finding that Myr treatment generally decreases the intracellular pool and the
70 rate of uptake of amino acids [22] raised the possibility that gradual sphingolipid depletion alters
71 the composition of amino acid transporters (AATs) at the PM. To explore this possibility, we
72 examined cells harboring chromosomal mNeonGreen (mNG) fusions to a panel of AAT genes
73 (*MUP1, CAN1, DIP5, LYP1, BAP3, GAP1*, and *TAT2*) in wildtype (SEY6210) and vacuolar Vph1-
74 mCherry-expressing background strains. Cells at mid-log phase were treated with Myr or mock-
75 treated (drug solvent) for 5 hours and mixed just prior to visualization by fluorescence microscopy.
76 Vph1-mCherry expression was used to identify cells that had been Myr-treated, while mock
77 treatment was performed on cells lacking any mCherry expression. Quantification of images was
78 performed by measuring mean fluorescence intensity at the PM of individual cells. Surprisingly,
79 Myr treatment did not alter PM levels of Can1, Dip5, and Lyp1, and slightly increased the levels
80 of Bap3 and Tat2 (**Fig. 1A-B**). Consistent with previously reported results, Myr-treated cells
81 exhibited decreased Mup1-mNG at the PM and increased Mup1-mNG flux into the vacuole (**Fig.
82 1A-B**), suggesting that sphingolipid depletion induces a selective endocytic clearance of the
83 methionine transporter, Mup1.

84

85 **Yeast cells respond to Myr by increasing abundance of specific glucose transporters**

86 Given that yeast cells respond to Myr by altering the PM composition of AATs we
87 considered the possibility that other nutrient transporters may also be affected. Specifically, given
88 the relationship between glucose metabolism and aging, we hypothesized that Myr treatment may
89 alter composition or activity of glucose transporters. To examine the effect of Myr on glucose
90 transport, yeast cells were incubated with radiolabeled ^{3}H-glucose and uptake was measured with
91 or without Myr treatment. Notably, glucose uptake was significantly lowered in cells treated with
92 Myr for at least 2 hours (**Fig. 2A**). To test if Myr treatment affects the abundance of glucose

93 transporters at the PM, we examined cells harboring chromosomal mNeonGreen (mNG) fusions
94 to a panel of hexose transporter genes (*HXT1, HXT2, HXT3, HXT6*) in wildtype (SEY6210) and
95 vacuolar Vph1-mCherry-expressing background strains. Cells were grown to mid-log phase,
96 treated with Myr or mock (drug solvent) for 5 hours and mixed just prior to visualization by
97 fluorescence microscopy (as described in **Fig. 1**). We found that Myr treatment had no effect on
98 the PM abundance of Hxt3 or Hxt6, while the low-affinity glucose transporter Hxt1 and the high-
99 affinity glucose transporter Hxt2 exhibited increased abundance at the PM (**Fig. 2B-C** and **Fig.**
100 **S2A-B**). Thus, Myr-treated cells selectively increase PM abundance of specific hexose
101 transporters, while experiencing decreased capacity for glucose uptake. These results are
102 unexpected and suggest impaired or suppressed activity of glucose transporters in sphingolipid-
103 depleted cells.

104 We expanded our analysis to include other categories of integral membrane proteins at
105 the PM. Importantly, Myr-treatment had negligible effects on the localization of the PM proton
106 pumps Pma1 and Pma2 as well as the cell wall stress sensor Wsc1 (**Fig. S3A**). Interestingly, Myr-
107 treated conferred PM stability to the pheromone receptor Ste2 and the ABD transporter Pdr5 (**Fig.**
108 **S3A**). We also observed an increase in PM association of several peripheral membrane proteins
109 that function in endocytosis, including several endocytic adaptors (Ent1, Ent2 and Ede1) (**Fig.**
110 **S3B-C**). The results of our analysis of how various PM proteins respond to Myr treatment are
111 summarized in **Table 1**.

112

113 **Myriocin decreases the bulk inflow of the PM**

114 It is noteworthy that several PM proteins accumulated at the PM following Myr treatment,
115 which we hypothesized may be due to a decrease in bulk endocytosis. To measure bulk
116 endocytosis, the lipophilic tracer dye FM4-64 (N-(3-triethylammoniumpropyl)-4-(p-
117 diethylaminophenylhexatrienyl) pyridium dibromide) was added to pulse-label the PM, followed
118 by washing and chasing for 1 hour. Bulk endocytosis results in most FM4-64 being delivered to

119 the limiting membrane of the vacuole (labelled by Vph1-mNG) in mock-treated cells (**Fig. S4A-B**
120 and **3A-B**). In contrast, cells treated with Myr for 4 hours exhibited reduced colocalization of FM4-
121 64 with Vph1-mNG (**Fig. 3A-B** and **Fig. S4C-D**), indicating a significant reduction in bulk
122 endocytosis. Notably, treatment of cells with Myr for 1 hour had no effect on bulk endocytosis,
123 while Myr treatment for 2 hours resulted in a partial but significant defect in bulk endocytosis (**Fig.**
124 **3A-B**). This defect in bulk endocytosis after 4 hours of Myr treatment likely contributes to the
125 accumulation of various PM proteins in the PM (**Table 1**). However, it is unclear how Myr triggers
126 the endocytic clearance of the high-affinity methionine permease Mup1 (**Fig. 1**) despite
127 impairment of bulk PM lipid endocytosis.
128
129 **Myriocin-induced trafficking of Mup1 requires the Rsp5 adaptor Art2**
130 To better understand how Myr triggers the endocytic clearance of Mup1, we first attempted
131 to validate our findings using yeast cells with chromosomal *MUP1* fused at its C-terminus to
132 superecliptic pHluorin, a GFP variant that does not fluoresce in the acidic environment of the
133 vacuole [23]. In this yeast variant, steady state levels of Mup1 at the PM can be measured by flow
134 cytometry [24]. Similar to our fluorescence microscopy results, this approach revealed Mup1
135 levels at the PM begin to decrease after 4 hours of Myr treatment (**Fig. 4A**). To test whether this
136 response is due to sphingolipid depletion, we analyzed the effect of Myr in cells cultured with
137 phytosphingosine (PHS)-supplemented media. Notably, the PHS supplementation prevents the
138 clearance of Mup1, indicating this response is the result of sphingolipid depletion (**Fig. 4B**).
139 Similar to Myr, aureobasidin (AbA), which inhibits the inositol phosphorylceramide synthase
140 AUR1, also triggered the clearance of Mup1, an effect which could not be reversed by PHS
141 supplementation (**Fig. 4C**). Taken together, these results reveal that PM clearance of Mup1 is
142 triggered by depletion of complex SLs which are synthesized downstream of ceramide (e.g.,
143 inositol phosphorylceramides and their mannosylated derivatives).

144 The endocytosis of nutrient transporters in yeast is controlled primarily by Rsp5-mediated
145 ubiquitylation events (reviewed in [25]). Pairing of the E3 ubiquitin ligase Rsp5 with cargo adaptors
146 called ARTs (arrestin-related trafficking adaptors) determines the specificity of substrate targeting
147 and promotes adaptation to nutrient fluctuations and stress conditions [26, 27]. Analysis of the
148 yeast transcriptional response to Myr treatment revealed increased transcript abundance for Rsp5
149 and several ARTs (**Fig. S5A**), indicating that sphingolipid depletion alters gene expression in a
150 way that could affect endocytic trafficking. For example, *ART1* and *ART2* were notably
151 upregulated in a Myr-treatment time course (**Fig. S5A-B**), and both are known to regulate Mup1
152 endocytosis in response to excess methionine [27, 28] and nitrogen starvation [29], respectively.
153 To test if ARTs are involved in this response, we characterized Myr-triggered Mup1-pHluorin
154 clearance in a panel of ART deletion yeast strains and found that all ARTs tested were
155 dispensable except for *ART2* (**Fig. 4D).** To validate this result, we performed fluorescence
156 microscopy to compare the PM abundance of Mup1-pHluorin in wildtype, *Δart1* or *Δart2* yeast
157 cells. Strikingly, Mup1 clearance was not detected in Myr-treated *Δart2* yeast cells, while loss of
158 ART1 did not affect this response (**Fig. 4E**). These findings indicate that Art2 mediates the
159 endocytic clearance of Mup1 in response to Myr treatment.
160

161 **Myr-induced trafficking of Mup1 requires Lys63-linked polyubiquitylation at its C-terminus**

162 Ubiquitylation at N-terminal lysines (K27 and K28) is required for Mup1 endocytosis in
163 response to excess methionine [30-32] while ubiquitylation at C-terminal lysines (K567 and K572)
164 is reported to mediate endocytic clearance in response to nitrogen starvation [29] (**Fig. 5A**). Since
165 Art1-mediated ubiquitylation of Mup1 occurs at N-terminal lysines (K27 and K28) and Art2 was
166 previously reported to bind at the C-terminus of Mup1 [29] we predicted that ubiquitylation of C-
167 terminal lysine residues may be required for Myr-induced endocytosis of Mup1. To test this
168 prediction we characterized Myr-induced trafficking of Mup1-mNG in strains with short C-terminal
169 truncations lacking one or both C-terminal lysine residues (ΔK572 and ΔK567ΔK572,

170 respectively) (**Fig. 5B**). While Mup1$^{\Delta K572}$-mNG exhibited Myr-induced endocytic clearance,
171 Mup1$^{\Delta K567\Delta K572}$-mNG was unresponsive to Myr treatment (**Fig. 5C-D**). These results indicate that
172 Myr-triggered Mup1 endocytosis requires ubiquitylation at its C-terminal lysine residues.
173 To measure the ubiquitylation of Mup1, we affinity purified Mup1-FLAG from yeast lysates
174 and analyzed it by SDS-PAGE and quantitative immunoblotting. This analysis revealed a
175 significant increase in K63-linked ubiquitin polymers associated with Mup1 in response to Myr
176 treatment (**Fig. 5E**). Previous work demonstrated that conjugation to monoubiquitin is sufficient
177 for Mup1 endocytosis in response to excess methionine [33]. In contrast, we found that yeast cells
178 expressing Ub^{K63R} as the sole source of ubiquitin were deficient for Myr-triggered endocytosis of
179 Mup1 (**Fig 5F** and **S5A-B**), indicating that K63-linked ubiquitin polymers are required for this
180 response. Taken together, our results reveal that Myr-induced endocytosis of Mup1 is ubiquitin-
181 mediated but proceeds by a mechanism that is distinct from methionine-induced endocytosis.
182
183 **Multiple ubiquitin-binding endocytic adaptors function in Myr-mediated Mup1 endocytosis**
184 Multiple ubiquitin-binding proteins in yeast, including the epsins Ent1 and Ent2 and the
185 epsin-like Ede1, function as adaptors that capture ubiquitylated cargoes during endocytic vesicle
186 formation. Among these, Ede1 was previously found to be crucial in mediating Mup1 trafficking in
187 response to excess methionine [34]. We observed an increased colocalization of Mup1-mNG with
188 Ent1-mCherry and Ent2-mNG, but not with Ede1, after 2.5 hours of Myr treatment (**Fig. 6A**).
189 However, a significant increase of Mup1-mNG colocalization with Ede1-mCherry occurred after 5
190 hours of Myr treatment (**Fig. 6B**). These results suggest that Mup1 association with all three
191 endocytic adaptors increases with variable kinetics during a Myr treatment time course. In
192 contrast, we did not observe any change in association between the arginine transporter Can1
193 and Ede1 during the same time course (**Fig. S6A**). To determine if the increased association
194 between Mup1 and Ede1 was due to ubiquitin binding, we analyzed association between Mup1-
195 mNG and a variant of Ede1 lacking its C-terminal UBA domain, which is known to preferentially

196 interact with K63-linked polymers [35]. Notably, the Ede1$^{\Delta uba}$ variant did not exhibit increased
197 association with Mup1 in response to Myr treatment (**Fig. 6C**). Taken together, our data suggest
198 that multiple endocytic adaptors contribute to Mup1 clearance in response to Myr treatment.
199
200

201 **Discussion**

202 Myriocin extends yeast chronological lifespan and our prior results revealed that this is
203 accomplished by establishing a state of amino acid restriction, which is accomplished at least in
204 part by decreasing the uptake of extracellular amino acids. Since our previous analysis revealed
205 that the high affinity methionine transporter undergoes Myr-induced endocytosis, we
206 hypothesized that other AATs would likewise be cleared from the PM following Myr treatment,
207 which would account for the broad decrease in the abundance of amino acids. Here, we report
208 the unexpected result that for almost all nutrient transporters and PM-associated proteins
209 examined Myr treatment induced either no change or increased abundance at the PM (**Table 1**).
210 The exception Mup1, which undergoes endocytic clearance following 4 hours of Myr treatment
211 (**Fig. 4**). These findings reveal that the decreased abundance of most amino acids observed
212 upon Myr treatment is not likely due to endocytic clearance of AATs, and in fact occurs despite
213 the increased PM abundance of Bap3 and Tat2. Thus, it is likely that the sphingolipid depletion
214 that occurs during Myr treatment lowers the transport activity of many AATs without inducing
215 endocytic clearance. Similar results were observed for hexose transporters, some of which
216 accumulated at the PM despite decreased glucose uptake during a Myr treatment time course. It
217 is possible the accumulation of specific PM proteins following Myr treatment is due to inhibition of
218 bulk endocytosis, which was observed using FM4-64 trafficking assays. Increased levels of
219 endocytic adaptors at the PM following Myr treatment suggests cargo capture and accumulation
220 of early endocytic intermediates which do not proceed to formation of vesicles, which is consistent
221 with the inhibition of bulk endocytosis. Alternatively, it is also possible that cells respond to
222 decreased amino acid and glucose availability by upregulating the biosynthesis and secretion of
223 specific nutrient transporters. Future studies will need to address why sphingolipid depletion
224 broadly decreases the activity of nutrient transporters at the PM.

225 The methionine transporter Mup1 was unique in that it was targeted for endocytic
226 clearance during a Myr treatment time course. Methionine-induced endocytosis of Mup1 is well-

227 characterized: it involves ubiquitylation of N-terminal lysine residues by the Art1-Rsp5 E3 ubiquitin
228 ligase complex, it occurs independently of ubiquitin polymer formation, and it requires the
229 endocytic adaptor Ede1. In contrast, we find that Myr-induced endocytosis of Mup1 is mediated
230 by the Art2-Rsp5 E3 ubiquitin ligase complex and it requires C-terminal lysine residues and the
231 formation of K63-linked ubiquitin polymers. Furthermore, Myr treatment induces co-localization of
232 Mup1 with Ent1 and Ent1 at early time points and with Ede1 at later time points – suggesting all
233 three endocytic adaptors contribute to Myr-mediated Mup1 clearance. Taken together, these
234 results reveal that Myr-mediated Mup1 endocytosis is mechanistically distinct from methionine-
235 mediated Mup1 endocytosis (**Fig. 7**). It remains unclear why Mup1 is selectively targeted for
236 endocytic clearance following sphingolipid depletion, and we hypothesize that altered methionine
237 homeostasis may be critical for Myr-mediated longevity. These findings shed new light on how
238 cells adapt to sphingolipid depletion and suggest that the regulation of methionine transport plays
239 a major role in determining yeast chronological life span.
240

241 **Materials and Methods**

242

243 **Strains, media and growth conditions**

244 *Saccharomyces cerevisiae* strains expressing endogenous reporter proteins fused with
245 fluorescent proteins were generated by homologous recombination or mating. Cells in synthetic
246 complete dextrose (SCD) media (preparation described in Hepowit et al. 2022) were grown at
247 26°C with agitation (220 rpm) to mid-log phase (OD600 = 0.3 – 0.6) and treated with 400 ng·mL^{-}
248 ^{1} myriocin (Cayman Chemical Company), Aureobasidin A (TaKaRa), phytosphingosine (Tokyo
249 Chemical Industry), or mock solution (95% ethanol) as needed. Cells expressing Hip1-mNG were
250 cultured in low-histidine SCD (2 µg·mL^{-1}), while strains expressing Hxt6-mNG and Hxt7-mNG
251 were grown in low-glucose SCD (0.2% glucose).

252

253 **Fluorescence Microscopy**

254 Yeast cells endogenously expressing fluorescent fusion proteins (mNG, MARS or mCherry) were
255 grown to mid-log phase in indicated SCD broth, treated with Myr for 5 h, concentrated by
256 centrifugation (3,500 X *g* for 10 s), and visualized using a DeltaVision Elite Imaging system
257 (Olympus IX-71 inverted microscope; Olympus 100× oil objective (1.4 NA); DV Elite sCMOS
258 camera, GE Healthcare). For the bulk endocytosis experiments using the 4-[6-[4-
259 (diethylamino)phenyl]-1,3,5-hexatrien-1-yl]-1-[3-(triethylammonio)propyl]-pyridiniumbromide dye
260 (FM 4-64, Invitrogen), the cells were prepared as previously described [36]. Fluorescence
261 colocalization was measured using Pearson correlation coefficients analyzed by the Softworx
262 software (GE Healthcare). Images obtained from the red and green filter channels were merged
263 and the background-subtracted mean fluorescence at the plasma membrane was measured
264 using Fiji [37].

265

266

267 **Flow Cytometry**

268 The endocytic trafficking of Mup1-pHluorin was analyzed using a flow cytometer as previously
269 described [22, 38] with minor modifications. Briefly, cells endogenously expressing Mup1-
270 pHluorin were grown to mid-log phase, treated with Myr or AbA, or in combination with PHS for 5
271 h, and analyzed using the BD Accuri^{TM} C6 Plus Flow Cytometer. The flow was set in fast fluidics
272 and the relative intensity of Mup1-pHluorin in 10,000 cells was measured in the FITC channel
273 using 90% histogram gating of the mock-treated cells for signal normalization.

274

275 **Western Blotting**

276 Endogenously expressed Mup1-FLAG was isolated by anti-FLAG immunoprecipitation as
277 previously described [39], dissolved in urea sample buffer containing 10% β-mercaptoethanol,
278 and resolved in 12% Bis-Tris PAGE gel by electrophoresis. Proteins were transferred onto PVDF
279 membrane (0.45 µm, GE Healthcare Amersham) by electrophoretic transblotting, blocked with
280 3% bovine serum albumin, and incubated with the following primary antibodies: anti-FLAG
281 (1:1,000; Sigma; Mab), anti-ubiquitin (1:10,000; LifeSensors; Mab; clone VU-1), anti-K63
282 (1:1,000; EMD Millipore, RAb; clone apu3). Secondary antibodies used were anti-mouse (IRDye
283 680RD-goat anti-mouse; LI-COR) and anti-rabbit (IRDye 800CW-goat anti-rabbit; LI-COR).
284 Fluorescence of blots was visualized using the Odyssey CLx Imaging System (LI-COR) and
285 quantified using Image Studio Lite (LI-COR).

286

287 **RNA seq analysis**

288 Total RNA was isolated from the lysate of 5 OD_{600} unit of cells, sampled every 1 h increment of
289 Myr treatment (up to 6 h), using the RNAeasy Mini Kit (Qiagen, Maryland). RNA samples were
290 frozen in dry-ice ethanol bath and stored at -80°C until use. RNA seq was performed at the J.
291 Carver Biotechnology Center at the University of Illinois and data are deposited in the Gene
292 Expression Omnibus (GSE199904; NCBI tracking system #22817261).

293

294

295 **Mass Spectrometry**

296 Comparative quantitation of different linkage types of ubiquitin polymers was performed using
297 SILAC-based mass spectrometry as previously described [38, 39] with minor modifications.
298 Briefly, cells in light Lys/Arg or heavy Lys/Arg synthetic media were grown to 0.3 OD_{600}, treated
299 with 400 ng·mL^{-1} Myr or the mock solution (95% ethanol) for 2 and 4 h, harvested by centrifugation
300 (3,500 X *g* for 5 min at 4°C), flush-frozen in liquid nitrogen, and stored at -80°C until use. Cells
301 were lysed in ice-cold lysis buffer (50 mM Tris-HCl [pH7.5], 150 mM NaCl, sodium pyrophosphate,
302 20 mM β-glycerophosphate, 2 mM sodium orthovanadate, 1 mM phenylmethylsulfonyl fluoride,
303 0.2% NP-40, 10 mM iodoacetamide, 20 μM MG132, 1 mM 1,10-phenanthroline, 1X EDTA-free
304 protease inhibitor cocktail [Roche], 1X PhosStop [Roche]) by bead beater agitation (3,000 rpm for
305 10 min with 1 min rest each interval) at 4°C. The whole-cell extract was clarified by centrifugation
306 at 21,000 X *g* for 10 min at 4°C, and the supernatant was diluted with equal volume of lysis buffer
307 without NP-40. Protein-conjugates of 3XFLAG-ubiquitin were isolated from the lysate by
308 immunoprecipitation using agarose bead slurry conjugated with anti-FLAG M2 (Sigma). After
309 washing the beads with ice-chilled TBS (50 mM Tris-HCl [pH7.5], 150 mM NaCl), the bound
310 proteins were eluted with 90 μL elution buffer (100 mM Tris-HCl [pH8.0], 1% SDS) at 98°C for
311 min. The eluted proteins were reduced with 10 mM DTT for 15 min at RT, alkylated with 20 mM
312 iodoacetamide (Sigma) in the dark for 30 min at RT, and precipitated with 300 μl PPT solution
313 (50% acetone, 49.9% ethanol, and 0.1% acetic acid). Precipitated proteins were washed with 200
314 μL PPT solution, sonicated for 30 s, centrifuged (21,000 X *g* for 10 min at 4°C) to separate the
315 pellet, and lyophilized by air-drying and quick vacuum centrifugation. Equal amounts of light and
316 heavy proteins were mixed, resolubilized in Urea-Tris solution (8 M urea, 50 mM Tris-HCl [pH8.0]),
317 diluted four-fold with MS-grade H_2O, and digested overnight with 1 μg MS-grade trypsin (Gold,
318 Promega) at 37°C. The 80 μL protein digest was acidified by adding 5 μL of 10% trifluoroacetic

319 acid (TFA) and 5 µL formic acid, clarified by centrifugation (21,000 X *g* for 1 min at RT), cleaned
320 by passing through a C18 column, lyophilized with a vacuum centrifuge (1 h at 45°C), and
321 dissolved in 12 µL 0.1% TFA. The peptides were loaded into a capillary reverse-phase analytical
322 column (360 µm O.D. X 100 µm I.D.) using a Dionex Ultimate 3000 nanoLC and autosampler,
323 and analyzed using a Q Exactive Plus mass spectrometer (Thermo Scientific). Ubiquitin chain
324 types were identified and quantified from resolved GlyGly-peptide footprints using MaxQuant (ver.
325 1.6.5.0).
326

Figure Legends

Figure. 1. Myr treatment selectively decreases the level of the primary methionine permease, Mup1, at the PM.

(A) Mixed population of yeast cells, expressing select mNG-tagged AATs, visualized under a fluorescence microscope after treatment with Myr (400 ng·mL^{-1}) or mock solution (95% ethanol). Vph1 is a vacuolar marker used to distinguish the two yeast populations in a mixture visualized at 0 h and 5 h after treatment.

(B) Quantification of the mean fluorescence intensity of select AAT-mNG at the PM, measured using Fiji (n = 30 - 60 cells; ±SD (error bars); triple asterisks (***) p value < 0.0005).

Figure 2. Myr increases the level of certain glucose transporters at the PM.

(A) Myr-treated cells have lower rate of ^{3}H-glucose uptake.

(B) Mixed population of yeast cells, expressing select mNG-tagged glucose transporters, visualized under a fluorescence microscope after treatment with Myr (400 ng·mL^{-1}) or mock solution (95% ethanol). Vph1 is a vacuolar marker used to distinguish the two yeast populations in a mixture visualized at 0 h and 5 h after treatment.

(C) Quantification of the mean fluorescence intensity of select glucose transporters (C-term tagged with mNG) at the PM, measured using Fiji (n = 30 - 60 cells; ±SD (error bars).

Figure 3. Myr inhibits the bulk endocytosis of PM lipids.

(A) Bulk endocytic trafficking of PM lipids and fusion with the vacuolar membrane. PM lipids were stained with a red lipophilic dye, FM 4-64, and vacuolar membrane was marked with green-fluorescing Vph1-mNG.

(B) Co-localization of FM 4-64 red fluorescence and Vph1-mNG green fluorescence measured as Pearson's Correlation Coefficient values using softWoRx (ver. 7.0.0).

Figure 4. Sphingolipid depletion induces the endocytic trafficking of Mup1, requiring the arrestin adaptor protein, Art2.

(A) Mup1-pHluorin fluorescence decreasing at the PM after 4 h of Myr treatment as measured by flow cytometry (n = 10,000 cells; ±SD (error bars)).

(B) Phytosphingosine supplementation stabilize Mup1-pHluorin at the PM (eight biological replicates; n = 10,000 cells; ±SD (error bars)).

(C) *ART2* is required in Myr-induced endocytic trafficking of Mup1-pHluorin. Mup1-pHluorin fluorescence signal at the PM of cells was measured by a flow cytometer (four biological replicates; n = 10,000 cells; ±SD (error bars)).

(D) Fluorescence microscopy showing that the *Δart2* null-deletion strain has stable Mup1-pHluorin signal at the PM after Myr treatment. Quantification is shown in Suppl. Fig. 4G.

Figure 5. Myr-induced trafficking of Mup1 requires K63-linked polyubiquitylation at the C-terminus of Mup1.

(A) Diagram showing the lysine residues at the cytosolic region of PM-associated Mup1.

(B) Diagram showing the C-terminal truncation variants of Mup1.

(C) Fluorescence microscopy of mixed cell populations (mNG-tagged Mup1 wt and truncation variants) after 5 h of Myr treatment.

(D) Quantification of Mup1-mNG expressed as mean fluorescence intensity at the PM of cells visualized in Fig. 5C.

(E) Anti-FLAG and anti-K63 polyUb immunoblots of Mup1-FLAG enriched by anti-FLAG immunoprecipitation after 2 or 4 h of Myr treatment.
(F) Flow cytometry of SUB280-derived cells (all four ubiquitin-coding genes deleted) that *trans*-express only the wt or K63R ubiquitin and endogenously expressing Mup1-pHluorin (four biological replicates; n = 10,000 cells; ±SD (error bars)).
(G) Fluorescence microscopy showing that SUB280 cells expressing only the Ub K63R have more stable Mup1-mNG signal at the PM after Myr treatment. Quantification is shown in Suppl. Fig. 5.

Figure 6. Myr treatment induces Mup1 colocalization with ubiquitin-binding early endocytic adaptor proteins.
(A) Colocalization of Mup1-pHluorin with Ent1-, Ent2-, and Ede1-mNG after 2 h of Myr treatment.
(B) Colocalization of Mup1-pHluorin with Ent1-, Ent2-, and Ede1-mNG after 4 h of Myr treatment.
(C) Myr-induced colocalization of Mup1 and Ede1 is abrogated when the UBA domain of Mup1 is deleted.

Figure 7. Comparison of Mup1 endocytic trafficking as induced by excess methionine and sphingolipid depletion.

Supplemental Figure Legends

Suppl. Fig 1. Quantification of mean fluorescence intensity of Bap1-, Gnp1-, and Hip1-mNG at the PM of cells after 5 h of Myr treatment (n = 20 cells; ±SD (error bars)).

Suppl. Fig. 2A. Fluorescence microscopy of mixed population of cells expressing endogenous Hxt1-mNG after Myr (SEY6210 wildtype cells) or mock solution (SEY6210 Vph1-MARS) treatment.

Suppl. Fig. 2B. Quantification of Hxt1-mNG fluorescence measurements obtained from fluorescence microscopy images (n = 20 cells; ±SD (error bars); subpopulation of cells presented in Suppl. Fig. 2A).

Suppl. Fig. 2C. Fluorescence microscopy of mixed population of cells endogenously expressing select AATs (C-term tagged with mNG) after Myr (SEY6210 Vph1-MARS) or mock solution (SEY6210 wildtype cells) treatment.

Suppl. Fig. 2D. Fluorescence microscopy of mixed population of cells endogenously expressing select early endocytic proteins (C-term tagged with mNG) after Myr (SEY6210 Vph1-MARS) or mock solution (SEY6210 wildtype cells) treatment.

Suppl. Fig. 2E-G. Quantification of the total fluorescence of cells expressing Pdr5-, Ede1-, or Abp1-mNG after Myr treatment.

Suppl. Fig. 3A. Bulk endocytic trafficking of FM 4-64-stained PM-derived lipids (red) and fusion with the vacuolar membranes (green, Vph1-mNG as marker).

Suppl. Fig. 3B. Myr treatment delays the rate of bulk PM lipid (red, stained with FM 4-64) endocytic trafficking as measured by its colocalization with the vacuolar membrane (green, Vph1-mNG as marker). Colocalization expressed as Pearson Correlation Coefficient values (n = 10 cells; ±SD (error bars). After 1 h of Myr treatment, cells were washed and resuspended in fresh SCD media and the bulk PM lipid trafficking was visualized after 0, 30, 60 min of incubation at 26°C.

Suppl. Fig. 3C. Fluorescence microscopy of BY4741 cells, showing that Myr inhibits the bulk endocytosis of PM lipids. PM was stained with FM 4-64 after 4 h of mock (95% EtOH) or Myr treatment.

Suppl. Fig. 3D. Quantification of the colocalization of FM 4-64 (red, PM-derived lipids) and Vph1-mNG (green, vacuolar membrane marker) expressed as Pearson Correlation Coefficient values (n = 20 cells; ±SD (error bars)).

Acknowledgements

We are grateful to T Graham, A Ebert, and S. Qualls-Histed for advice and helpful discussions. NLH and JAM were supported by NIH grant R35 GM144112 (to JAM).

Conflicts of Interest

The authors declare no conflicts of interest.

References

1. Körner C, Fröhlich F. Compartmentation and functions of sphingolipids. Curr Opin Cell Biol. 2022;74:104-11. Epub 20220225. doi: 10.1016/j.ceb.2022.01.006. PubMed PMID: 35228099.
2. Deng Y, Pakdel M, Blank B, Sundberg EL, Burd CG, von Blume J. Activity of the SPCA1 Calcium Pump Couples Sphingomyelin Synthesis to Sorting of Secretory Proteins in the Trans-Golgi Network. Dev Cell. 2018;47(4):464-78.e8. Epub 20181101. doi: 10.1016/j.devcel.2018.10.012. PubMed PMID: 30393074; PubMed Central PMCID: PMCPMC6261503.
3. Sundberg EL, Deng Y, Burd CG. Syndecan-1 Mediates Sorting of Soluble Lipoprotein Lipase with Sphingomyelin-Rich Membrane in the Golgi Apparatus. Dev Cell. 2019;51(3):387-98.e4. Epub 20190919. doi: 10.1016/j.devcel.2019.08.014. PubMed PMID: 31543446; PubMed Central PMCID: PMCPMC6832887.
4. Cartier A, Hla T. Sphingosine 1-phosphate: Lipid signaling in pathology and therapy. Science. 2019;366(6463). doi: 10.1126/science.aar5551. PubMed PMID: 31624181; PubMed Central PMCID: PMCPMC7661103.
5. Berchtold D, Piccolis M, Chiaruttini N, Riezman I, Riezman H, Roux A, et al. Plasma membrane stress induces relocalization of Slm proteins and activation of TORC2 to promote sphingolipid synthesis. Nat Cell Biol. 2012;14(5):542-7. Epub 20120415. doi: 10.1038/ncb2480. PubMed PMID: 22504275.
6. Kalinichenko LS, Gulbins E, Kornhuber J, Müller CP. Sphingolipid control of cognitive functions in health and disease. Prog Lipid Res. 2022;86:101162. Epub 20220319. doi: 10.1016/j.plipres.2022.101162. PubMed PMID: 35318099.
7. Janneh AH, Ogretmen B. Targeting Sphingolipid Metabolism as a Therapeutic Strategy in Cancer Treatment. Cancers (Basel). 2022;14(9). Epub 20220427. doi: 10.3390/cancers14092183. PubMed PMID: 35565311; PubMed Central PMCID: PMCPMC9104917.
8. Bataller M, Sánchez-García A, Garcia-Mayea Y, Mir C, Rodriguez I, LLeonart ME. The Role of Sphingolipids Metabolism in Cancer Drug Resistance. Front Oncol. 2021;11:807636. Epub 20211223. doi: 10.3389/fonc.2021.807636. PubMed PMID: 35004331; PubMed Central PMCID: PMCPMC8733468.
9. Huang X, Withers BR, Dickson RC. Sphingolipids and lifespan regulation. Biochim Biophys Acta. 2014;1841(5):657-64. Epub 20130815. doi: 10.1016/j.bbalip.2013.08.006. PubMed PMID: 23954556; PubMed Central PMCID: PMCPMC3925463.
10. Glaros EN, Kim WS, Garner B. Myriocin-mediated up-regulation of hepatocyte apoA-I synthesis is associated with ERK inhibition. Clin Sci (Lond). 2010;118(12):727-36. Epub 2010/01/28. doi: CS20090452 [pii]
10.1042/CS20090452. PubMed PMID: 20102334; PubMed Central PMCID: PMC2860698.
11. Jiang XC, Goldberg IJ, Park TS. Sphingolipids and cardiovascular diseases: lipoprotein metabolism, atherosclerosis and cardiomyopathy. Adv Exp Med Biol. 2011;721:19-39. Epub 2011/09/13. doi: 10.1007/978-1-4614-0650-1_2. PubMed PMID: 21910080.
12. Yu Z, Peng Q, Li S, Hao H, Deng J, Meng L, et al. Myriocin and d-PDMP ameliorate atherosclerosis in ApoE-/- mice via reducing lipid uptake and vascular inflammation. Clin Sci (Lond). 2020;134(5):439-58. Epub 2020/02/25. doi: 10.1042/CS20191028. PubMed PMID: 32091078.
13. Summers SA, Chaurasia B, Holland WL. Metabolic Messengers: ceramides. Nat Metab. 2019;1(11):1051-8. Epub 2020/07/23. doi: 10.1038/s42255-019-0134-8. PubMed PMID: 32694860.
14. Aburasayn H, Al Batran R, Ussher JR. Targeting ceramide metabolism in obesity. Am J Physiol Endocrinol Metab. 2016;311(2):E423-35. Epub 2016/07/07. doi: 10.1152/ajpendo.00133.2016. PubMed PMID: 27382035.
15. Yaguchi M, Shibata S, Satomi Y, Hirayama M, Adachi R, Asano Y, et al. Antitumor activity of a novel and orally available inhibitor of serine palmitoyltransferase. Biochem Biophys Res Commun. 2017. doi: 10.1016/j.bbrc.2017.01.075. PubMed PMID: 28108287.

498 16. Selwan EM, Finicle BT, Kim SM, Edinger AL. Attacking the supply wagons to starve cancer cells to
499 death. FEBS Lett. 2016;590(7):885-907. doi: 10.1002/1873-3468.12121. PubMed PMID: 26938658;
500 PubMed Central PMCID: PMCPMC4833639.
501 17. Woo CY, Baek JY, Kim AR, Hong CH, Yoon JE, Kim HS, et al. Inhibition of Ceramide Accumulation in
502 Podocytes by Myriocin Prevents Diabetic Nephropathy. Diabetes Metab J. 2019;44(4):581-91. Epub
503 2019/11/09. doi: 10.4093/dmj.2019.0063. PubMed PMID: 31701696.
504 18. Appriou Z, Nay K, Pierre N, Saligaut D, Lefeuvre-Orfila L, Martin B, et al. Skeletal muscle ceramides
505 do not contribute to physical-inactivity-induced insulin resistance. Appl Physiol Nutr Metab.
506 2019;44(11):1180-8. Epub 2019/03/20. doi: 10.1139/apnm-2018-0850. PubMed PMID: 30889368.
507 19. Geekiyanage H, Upadhye A, Chan C. Inhibition of serine palmitoyltransferase reduces Abeta and
508 tau hyperphosphorylation in a murine model: a safe therapeutic strategy for Alzheimer's disease.
509 Neurobiol Aging. 2013;34(8):2037-51. Epub 2013/03/27. doi: S0197-4580(13)00063-8 [pii]
510 10.1016/j.neurobiolaging.2013.02.001. PubMed PMID: 23528227; PubMed Central PMCID: PMC3651806.
511 20. Petit CS, Lee JJ, Boland S, Swarup S, Christiano R, Lai ZW, et al. Inhibition of sphingolipid synthesis
512 improves outcomes and survival in GARP mutant wobbler mice, a model of motor neuron degeneration.
513 Proc Natl Acad Sci USA. 2020;117(19):10565-74. Epub 2020/04/30. doi: 10.1073/pnas.1913956117.
514 PubMed PMID: 32345721; PubMed Central PMCID: PMCPMC7229683.
515 21. Lin G, Wang L, Marcogliese PC, Bellen HJ. Sphingolipids in the Pathogenesis of Parkinson's Disease
516 and Parkinsonism. Trends Endocrinol Metab. 2019;30(2):106-17. Epub 2018/12/12. doi:
517 10.1016/j.tem.2018.11.003. PubMed PMID: 30528460.
518 22. Hepowit NL, Macedo JKA, Young LEA, Liu K, Sun RC, MacGurn JA, et al. Enhancing lifespan of
519 budding yeast by pharmacological lowering of amino acid pools. Aging (Albany NY). 2021;13(6):7846-71.
520 Epub 20210321. doi: 10.18632/aging.202849. PubMed PMID: 33744865; PubMed Central PMCID:
521 PMCPMC8034917.
522 23. Prosser DC, Whitworth K, Wendland B. Quantitative analysis of endocytosis with cytoplasmic
523 pHluorin chimeras. Traffic. 2010;11(9):1141-50. doi: 10.1111/j.1600-0854.2010.01088.x. PubMed PMID:
524 20626707; PubMed Central PMCID: PMCPMC2919640.
525 24. Lee S, Ho HC, Tumolo JM, Hsu PC, MacGurn JA. Methionine triggers Ppz-mediated
526 dephosphorylation of Art1 to promote cargo-specific endocytosis. J Cell Biol. 2019. Epub 2019/01/04. doi:
527 10.1083/jcb.201712144. PubMed PMID: 30610170.
528 25. Lauwers E, Erpapazoglou Z, Haguenauer-Tsapis R, André B. The ubiquitin code of yeast permease
529 trafficking. Trends Cell Biol. 2010;20(4):196-204. doi: 10.1016/j.tcb.2010.01.004. PubMed PMID:
530 20138522.
531 26. Kahlhofer J, Leon S, Teis D, Schmidt O. The α-arrestin family of ubiquitin ligase adaptors links
532 metabolism with selective endocytosis. Biol Cell. 2021;113(4):183-219. Epub 20210201. doi:
533 10.1111/boc.202000137. PubMed PMID: 33314196.
534 27. Lin CH, MacGurn JA, Chu T, Stefan CJ, Emr SD. Arrestin-related ubiquitin-ligase adaptors regulate
535 endocytosis and protein turnover at the cell surface. Cell. 2008;135(4):714-25. Epub 20081030. doi:
536 10.1016/j.cell.2008.09.025. PubMed PMID: 18976803.
537 28. MacGurn JA, Hsu PC, Smolka MB, Emr SD. TORC1 regulates endocytosis via Npr1-mediated
538 phosphoinhibition of a ubiquitin ligase adaptor. Cell. 2011;147(5):1104-17. doi:
539 10.1016/j.cell.2011.09.054. PubMed PMID: 22118465.
540 29. Ivashov V, Zimmer J, Schwabl S, Kahlhofer J, Weys S, Gstir R, et al. Complementary α-arrestin-
541 ubiquitin ligase complexes control nutrient transporter endocytosis in response to amino acids. Elife.
542 2020;9. Epub 20200803. doi: 10.7554/eLife.58246. PubMed PMID: 32744498; PubMed Central PMCID:
543 PMCPMC7449699.

544 30. Guiney EL, Klecker T, Emr SD. Identification of the endocytic sorting signal recognized by the Art1-
545 Rsp5 ubiquitin ligase complex. Mol Biol Cell. 2016;27(25):4043-54. Epub 20161019. doi:
546 10.1091/mbc.E16-08-0570. PubMed PMID: 27798240; PubMed Central PMCID: PMCPMC5156545.
547 31. Busto JV, Elting A, Haase D, Spira F, Kuhlman J, Schäfer-Herte M, et al. Lateral plasma membrane
548 compartmentalization links protein function and turnover. EMBO J. 2018;37(16). Epub 20180705. doi:
549 10.15252/embj.201899473. PubMed PMID: 29976762; PubMed Central PMCID: PMCPMC6092676.
550 32. Ghaddar K, Merhi A, Saliba E, Krammer EM, Prévost M, André B. Substrate-induced ubiquitylation
551 and endocytosis of yeast amino acid permeases. Mol Cell Biol. 2014;34(24):4447-63. Epub 20140929. doi:
552 10.1128/MCB.00699-14. PubMed PMID: 25266656; PubMed Central PMCID: PMCPMC4248734.
553 33. Stringer DK, Piper RC. A single ubiquitin is sufficient for cargo protein entry into MVBs in the
554 absence of ESCRT ubiquitination. J Cell Biol. 2011;192(2):229-42. Epub 20110117. doi:
555 10.1083/jcb.201008121. PubMed PMID: 21242292; PubMed Central PMCID: PMCPMC3172180.
556 34. Wrasman K, Alioto SL, Zhang Y, Hoban K, Khairy M, Goode BL, et al. A Flow Cytometry-Based
557 Phenotypic Screen To Identify Novel Endocytic Factors in. G3 (Bethesda). 2018;8(5):1497-512. Epub
558 20180504. doi: 10.1534/g3.118.200102. PubMed PMID: 29540444; PubMed Central PMCID:
559 PMCPMC5940143.
560 35. Sims JJ, Haririnia A, Dickinson BC, Fushman D, Cohen RE. Avid interactions underlie the Lys63-
561 linked polyubiquitin binding specificities observed for UBA domains. Nat Struct Mol Biol. 2009;16(8):883-
562 9. Epub 20090720. doi: 10.1038/nsmb.1637. PubMed PMID: 19620964; PubMed Central PMCID:
563 PMCPMC2744598.
564 36. Tumolo JM, Hepowit NL, Joshi SS, MacGurn JA. A Snf1-related nutrient-responsive kinase
565 antagonizes endocytosis in yeast. PLoS Genet. 2020;16(3):e1008677. Epub 20200319. doi:
566 10.1371/journal.pgen.1008677. PubMed PMID: 32191698; PubMed Central PMCID: PMCPMC7176151.
567 37. Schindelin J, Arganda-Carreras I, Frise E, Kaynig V, Longair M, Pietzsch T, et al. Fiji: an open-source
568 platform for biological-image analysis. Nat Methods. 2012;9(7):676-82. Epub 20120628. doi:
569 10.1038/nmeth.2019. PubMed PMID: 22743772; PubMed Central PMCID: PMCPMC3855844.
570 38. Lee S, Ho HC, Tumolo JM, Hsu PC, MacGurn JA. Methionine triggers Ppz-mediated
571 dephosphorylation of Art1 to promote cargo-specific endocytosis. J Cell Biol. 2019;218(3):977-92. Epub
572 20190104. doi: 10.1083/jcb.201712144. PubMed PMID: 30610170; PubMed Central PMCID:
573 PMCPMC6400557.
574 39. Hepowit NL, Pereira KN, Tumolo JM, Chazin WJ, MacGurn JA. Identification of ubiquitin Ser57
575 kinases regulating the oxidative stress response in yeast. Elife. 2020;9. Epub 20201019. doi:
576 10.7554/eLife.58155. PubMed PMID: 33074099; PubMed Central PMCID: PMCPMC7647399.
577

Figure 1

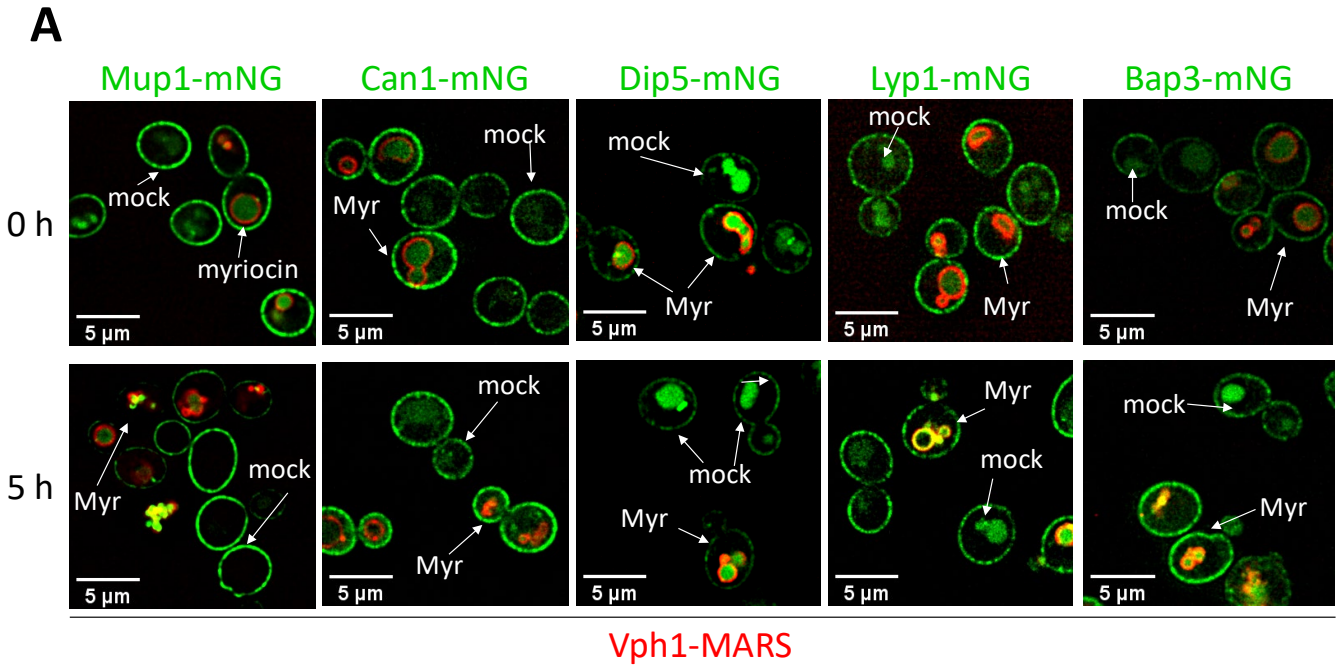
A
Mup1-mNG
Can1-mNG
Dip5-mNG
Lyp1-mNG
Bap3-mNG
0 h
5 h
mock
myriocin
Myr
5 µm
Vph1-MARS

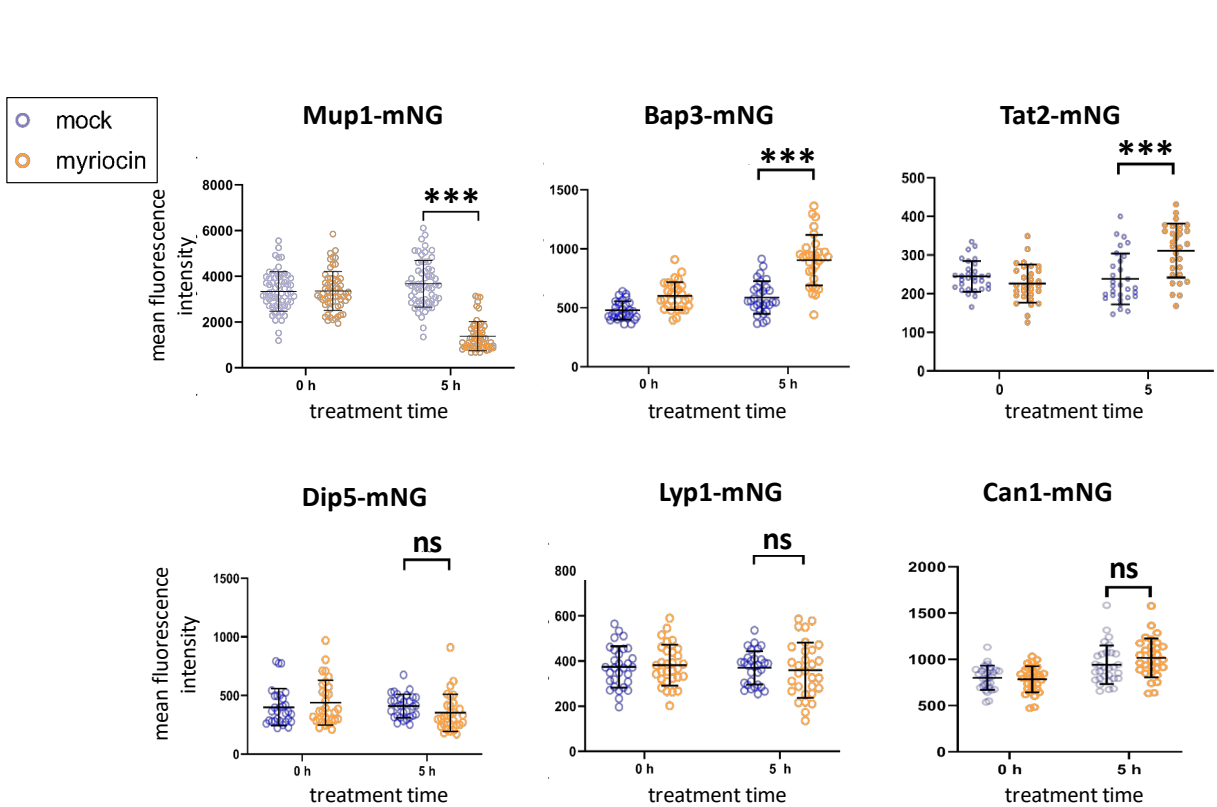
B
mock
myriocin
Mup1-mNG
Bap3-mNG
Tat2-mNG
Dip5-mNG
Lyp1-mNG
Can1-mNG
***
ns
mean fluorescence intensity
treatment time
0 h
5 h

Figure 2

A

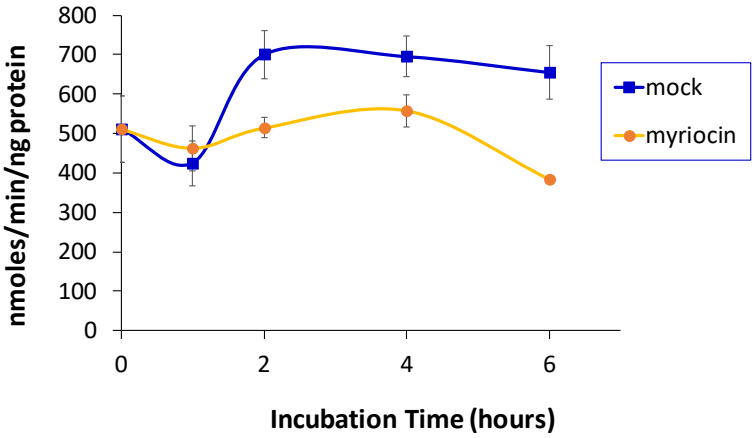
nmoles/min/ng protein
800
700
600
500
400
300
200
100
0
0
2
4
6
Incubation Time (hours)
mock
myriocin

B

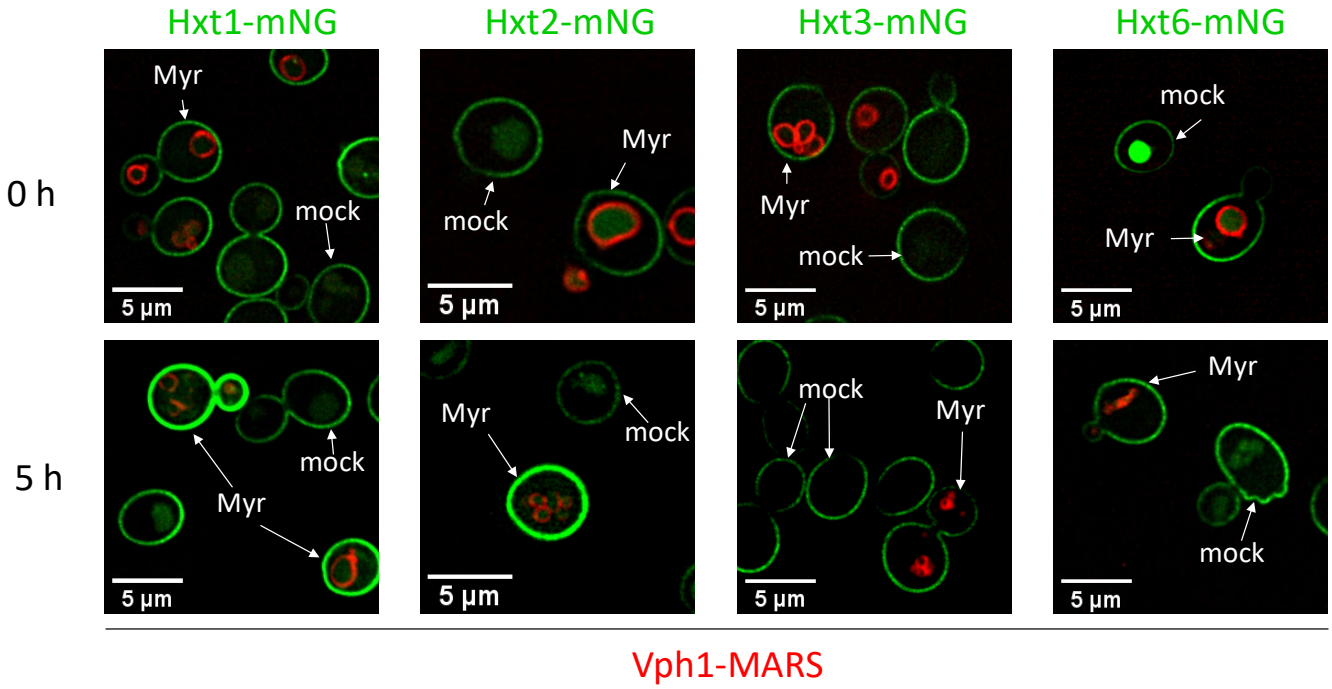
Hxt1-mNG
Hxt2-mNG
Hxt3-mNG
Hxt6-mNG
0 h
5 h
Myr
mock
5 µm
Vph1-MARS

C

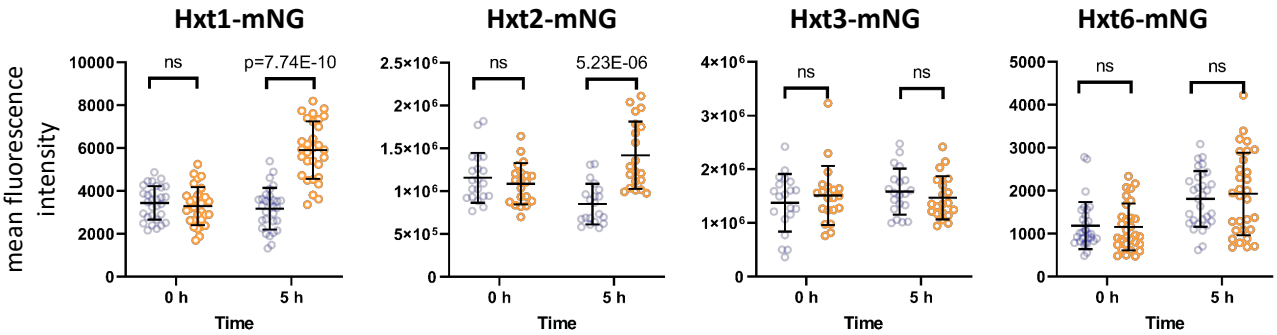
Hxt1-mNG
Hxt2-mNG
Hxt3-mNG
Hxt6-mNG
mean fluorescence intensity
ns
p=7.74E-10
5.23E-06
0 h
5 h
Time

Figure 3

A

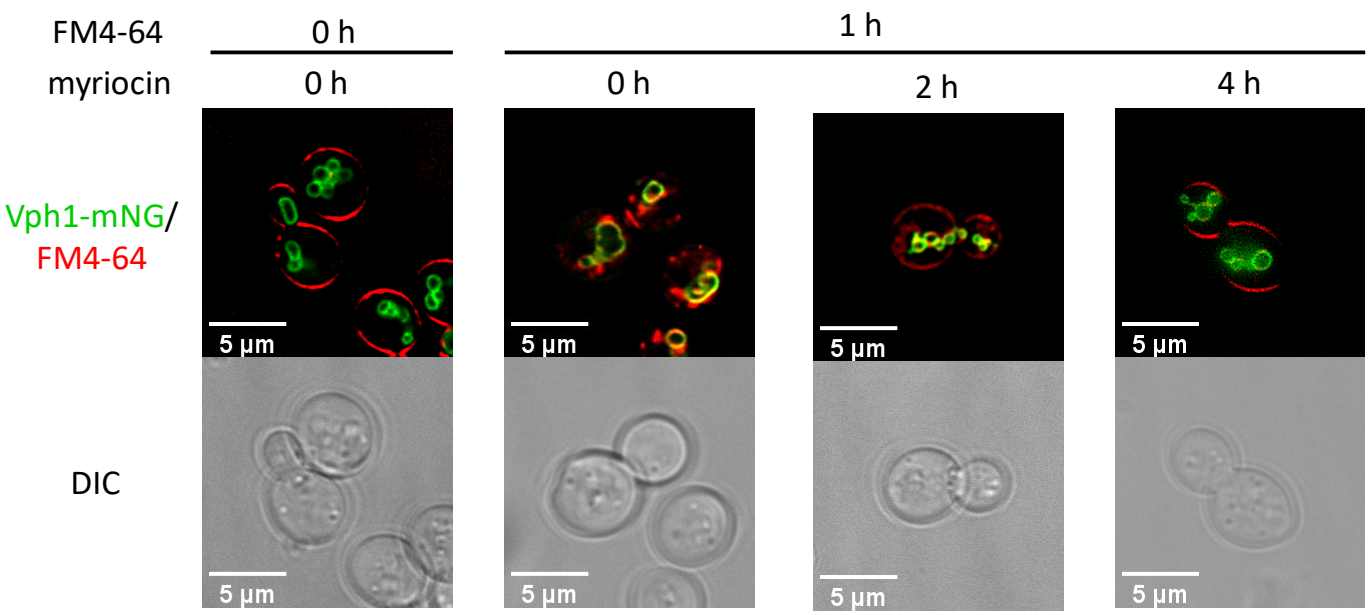
FM4-64
0 h
1 h
myriocin
0 h
0 h
2 h
4 h
Vph1-mNG/
FM4-64
DIC
5 µm

B

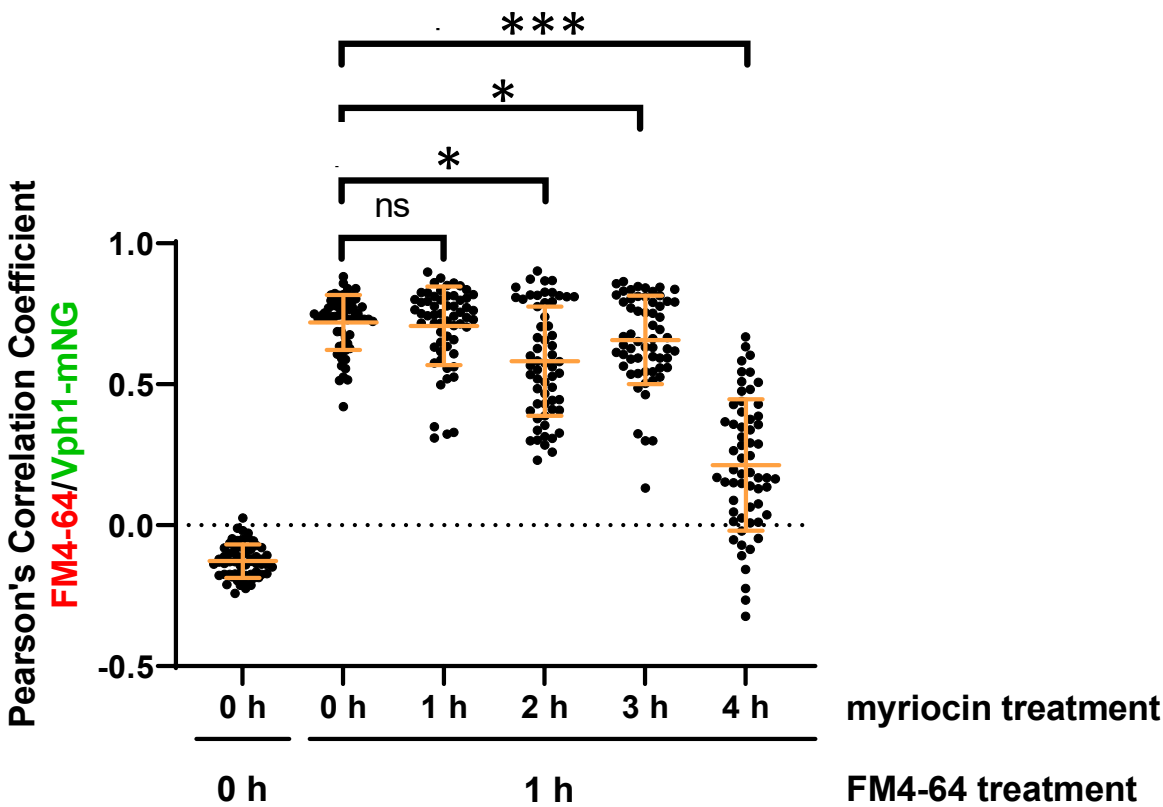
***
*
*
ns
Pearson's Correlation Coefficient
FM4-64/Vph1-mNG
1.0
0.5
0.0
-0.5
0 h
0 h
1 h
2 h
3 h
4 h
myriocin treatment
0 h
1 h
FM4-64 treatment

Figure 4

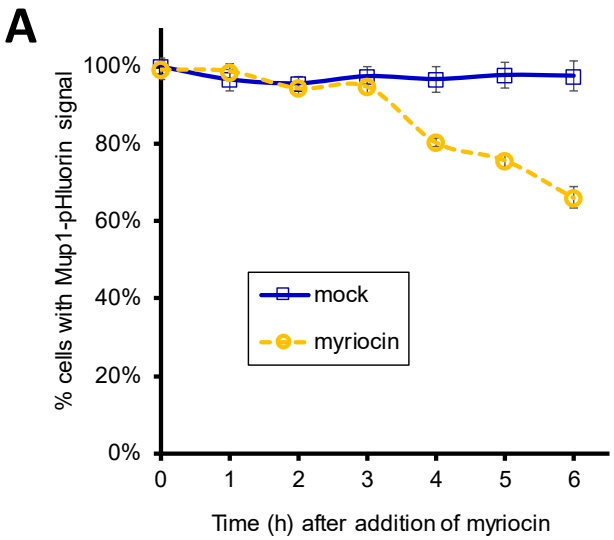
A
100%
80%
60%
40%
20%
0%
% cells with Mup1-pHluorin signal
mock
myriocin
0
1
2
3
4
5
6
Time (h) after addition of myriocin

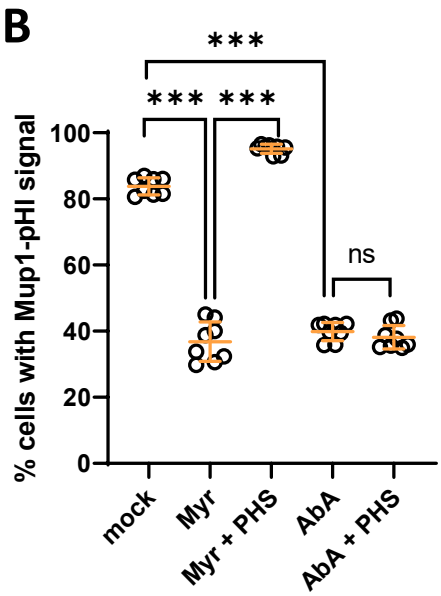
B
***
***
***
ns
100
80
60
40
20
0
% cells with Mup1-pHl signal
mock
Myr
Myr + PHS
AbA
AbA + PHS

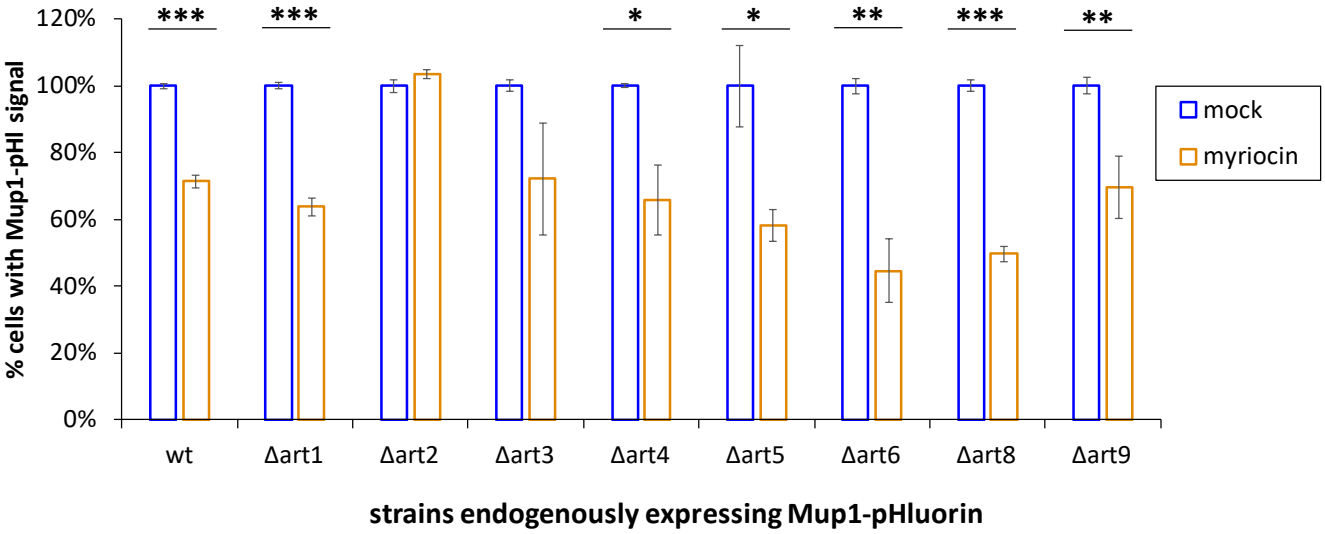
C
120%
100%
80%
60%
40%
20%
0%
% cells with Mup1-pHl signal
***
***
*
*
**
***
**
mock
myriocin
wt
Δart1
Δart2
Δart3
Δart4
Δart5
Δart6
Δart8
Δart9
strains endogenously expressing Mup1-pHluorin

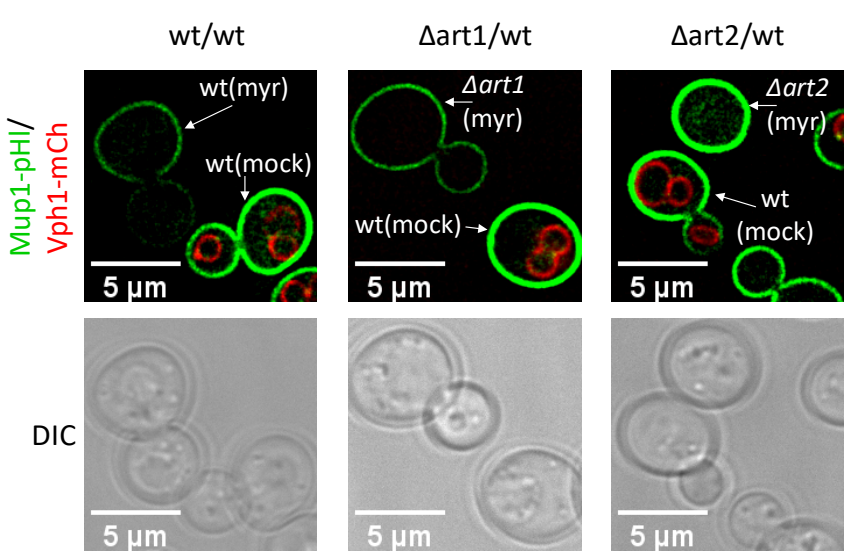
D
wt/wt
Δart1/wt
Δart2/wt
Mup1-pHl/
Vph1-mCh
wt(myr)
wt(mock)
Δart1
(myr)
wt(mock)
Δart2
(myr)
wt
(mock)
5 µm
DIC
5 µm

Figure 5

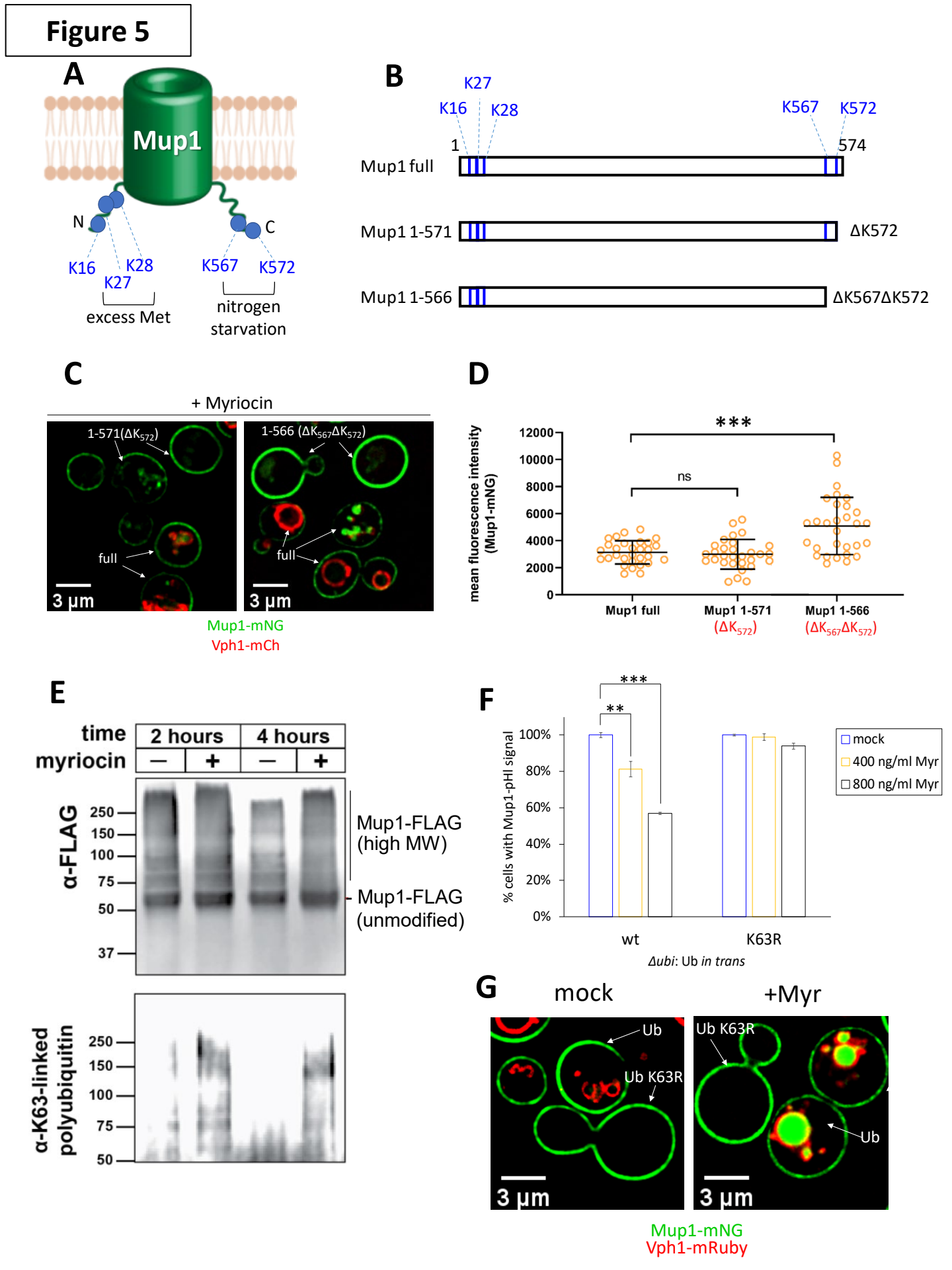
A
Mup1
N
C
K16
K28
K27
K567
K572
excess Met
nitrogen starvation
B
K27
K16
K28
K567
K572
1
574
Mup1 full
Mup1 1-571
ΔK572
Mup1 1-566
ΔK567ΔK572
C
+ Myriocin
1-571(ΔK572)
1-566 (ΔK567ΔK572)
full
full
3 µm
3 µm
Mup1-mNG
Vph1-mCh
D
mean fluorescence intensity (Mup1-mNG)
12000
10000
8000
6000
4000
2000
0
***
ns
Mup1 full
Mup1 1-571 (ΔK572)
Mup1 1-566 (ΔK567ΔK572)
E
time
2 hours
4 hours
myriocin
—
+
—
+
α-FLAG
250
150
100
75
50
37
Mup1-FLAG (high MW)
Mup1-FLAG (unmodified)
α-K63-linked polyubiquitin
250
150
100
75
50
F
% cells with Mup1-pHl signal
100%
80%
60%
40%
20%
0%
***
**
mock
400 ng/ml Myr
800 ng/ml Myr
wt
K63R
Δubi: Ub in trans
G
mock
+Myr
Ub
Ub K63R
Ub K63R
Ub
3 µm
3 µm
Mup1-mNG
Vph1-mRuby

Figure 6

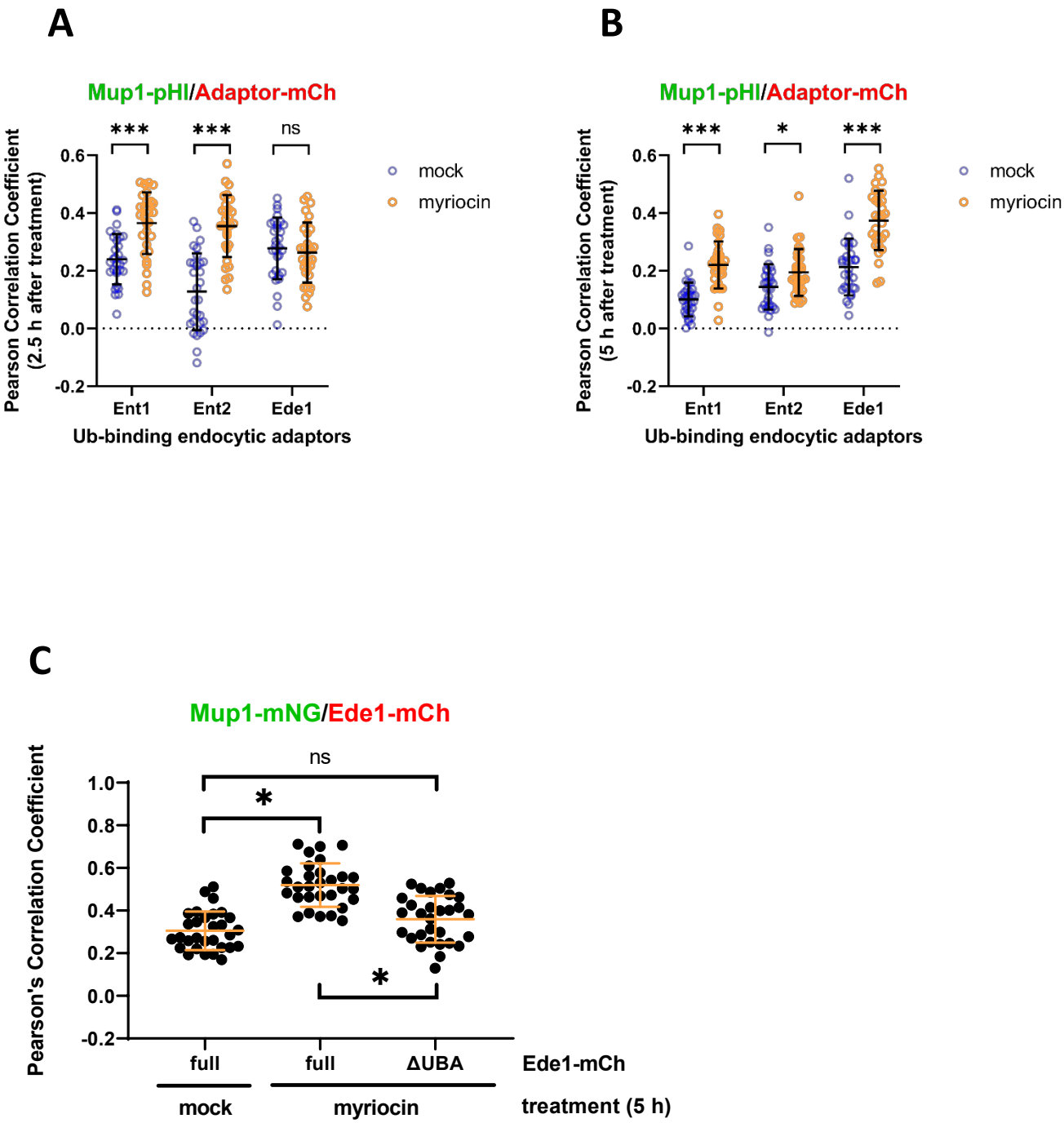
A
Mup1-pHl/Adaptor-mCh
Pearson Correlation Coefficient (2.5 h after treatment)
***
***
ns
0.6
0.4
0.2
0.0
-0.2
Ent1
Ent2
Ede1
Ub-binding endocytic adaptors
mock
myriocin
B
Mup1-pHl/Adaptor-mCh
Pearson Correlation Coefficient (5 h after treatment)
***
*
***
0.6
0.4
0.2
0.0
-0.2
Ent1
Ent2
Ede1
Ub-binding endocytic adaptors
mock
myriocin
C
Mup1-mNG/Ede1-mCh
Pearson's Correlation Coefficient
ns
*
*
1.0
0.8
0.6
0.4
0.2
0.0
-0.2
full
full
ΔUBA
Ede1-mCh
mock
myriocin
treatment (5 h)

Figure 7

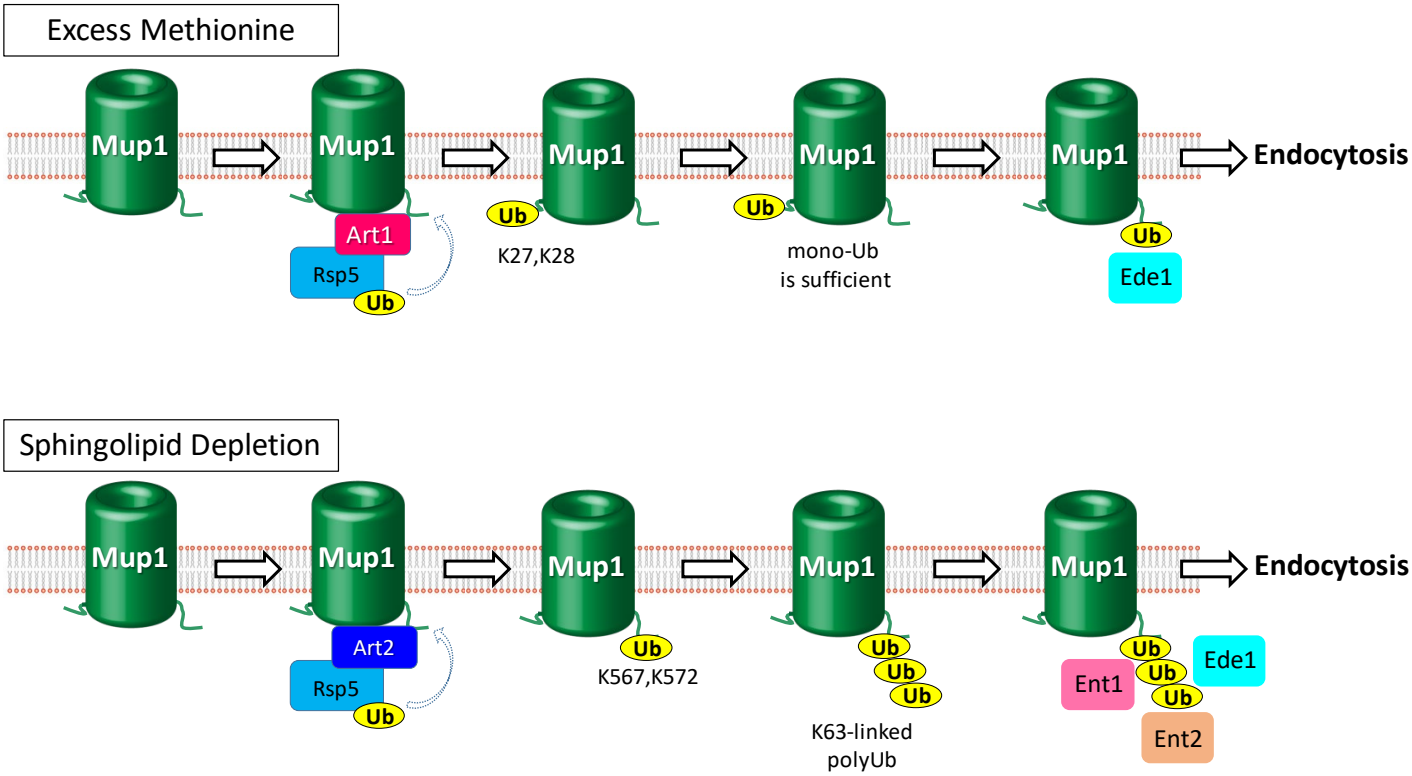
Excess Methionine
Mup1
Mup1
Art1
Rsp5
Ub
Mup1
Ub
K27,K28
Mup1
Ub
mono-Ub
is sufficient
Mup1
Ub
Ede1
Endocytosis
Sphingolipid Depletion
Mup1
Mup1
Art2
Rsp5
Ub
Mup1
Ub
K567,K572
Mup1
Ub
Ub
Ub
K63-linked
polyUb
Mup1
Ub
Ub
Ub
Ub
Ent1
Ede1
Ent2
Endocytosis

Suppl. Fig. 1

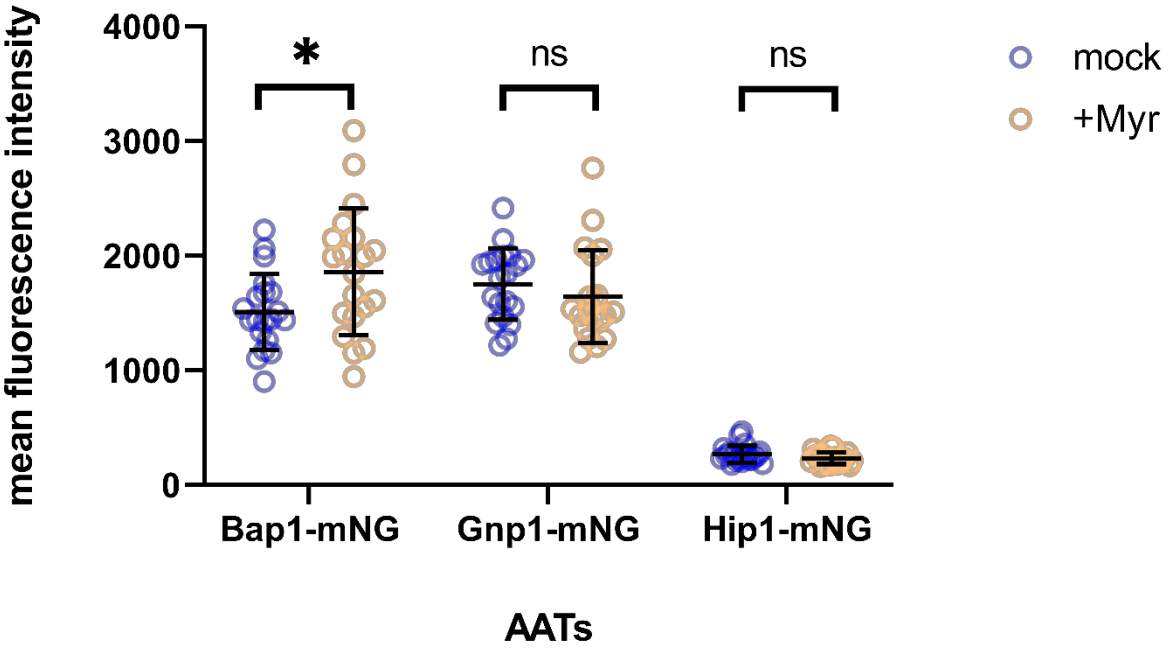
mean fluorescence intensity
4000
3000
2000
1000
0
*
ns
ns
mock
+Myr
Bap1-mNG
Gnp1-mNG
Hip1-mNG
AATs

Suppl. Fig. 2A

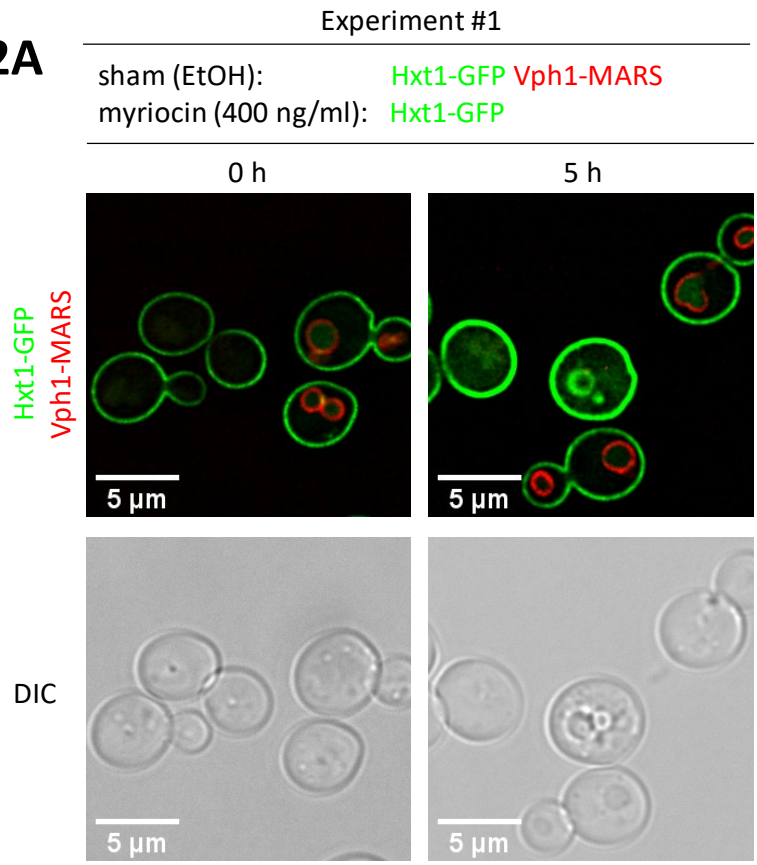

Suppl. Fig. 2B

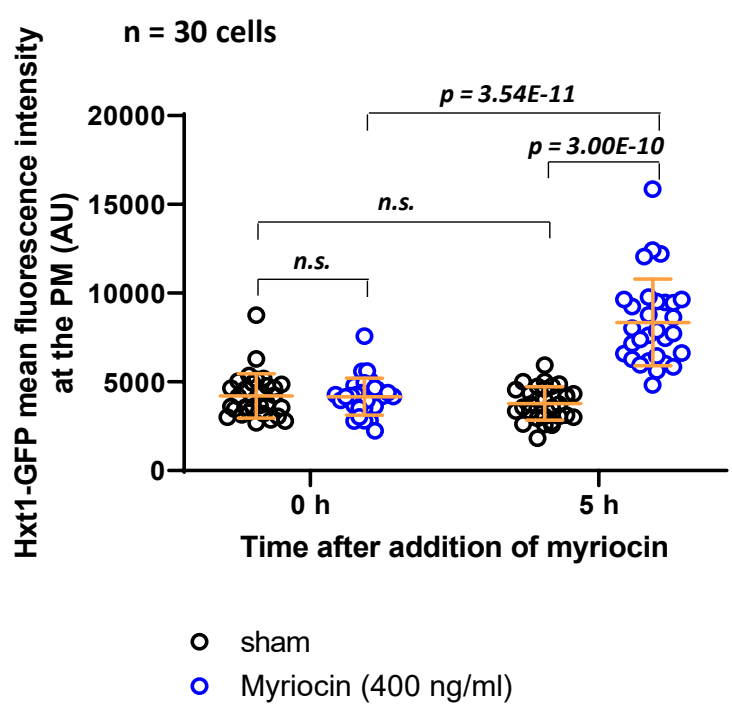

Suppl. Fig. 2C

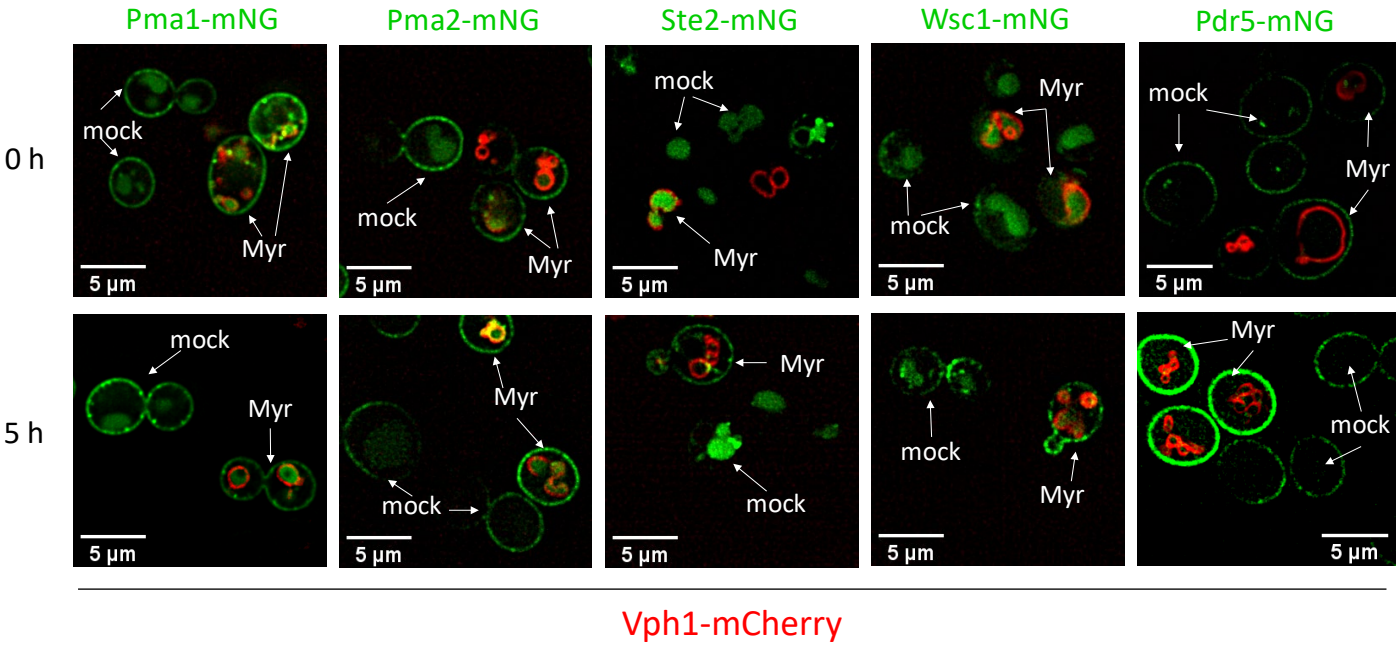

Suppl. Fig. 2D

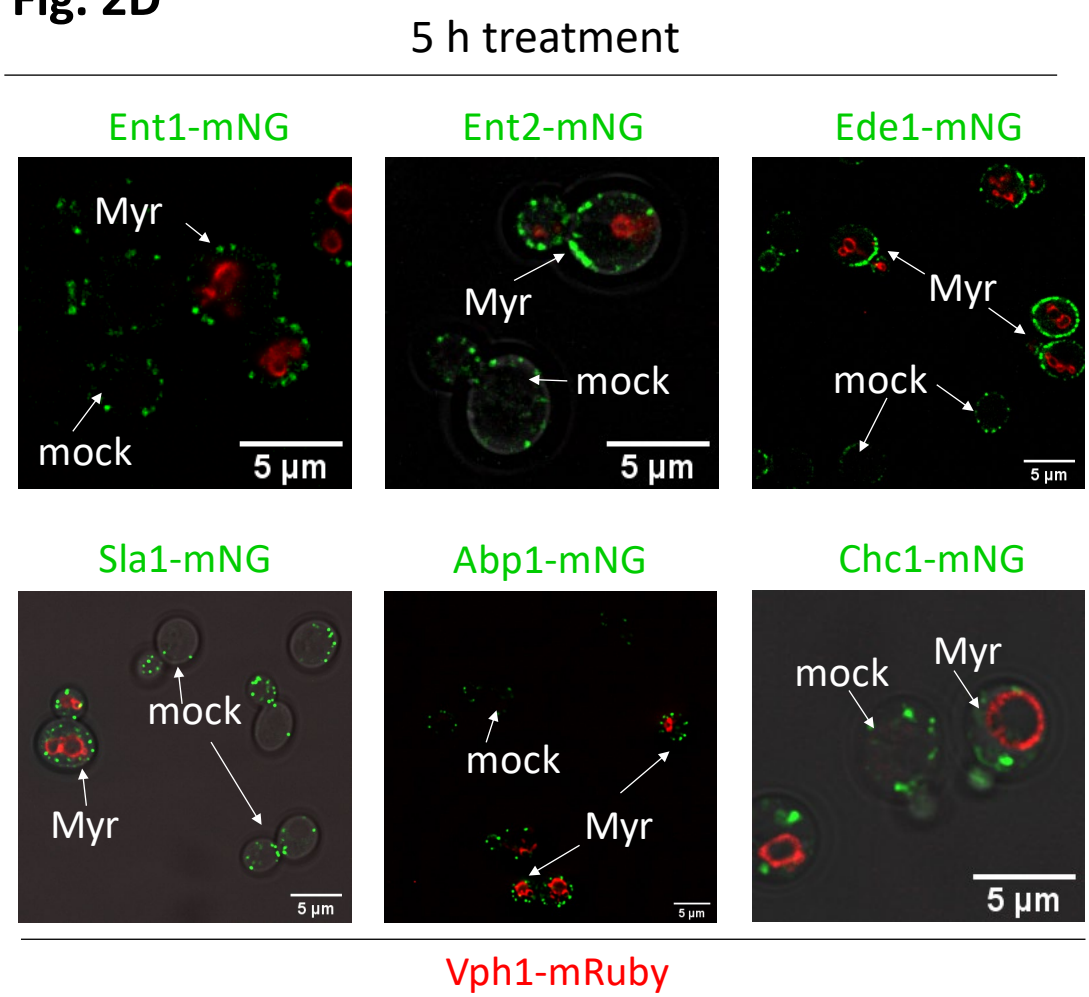

Suppl. Fig. 2E

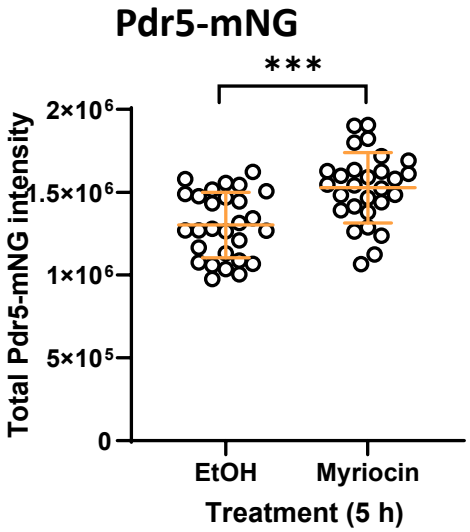

Suppl. Fig. 2F

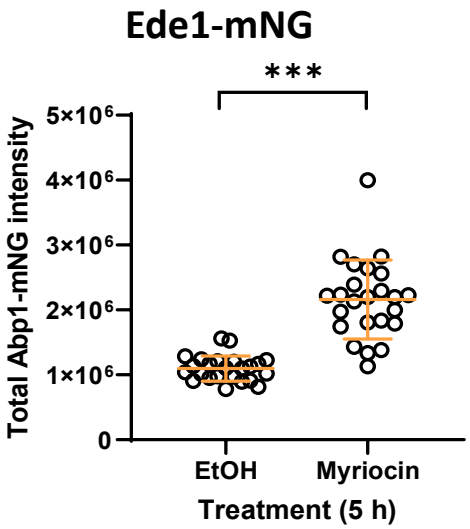

Suppl. Fig. 2G

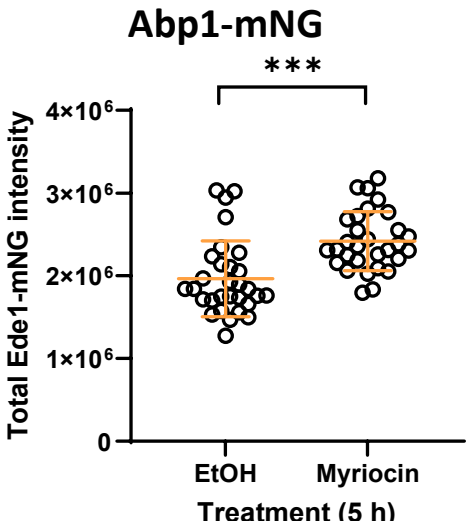

Suppl. Fig. 3A

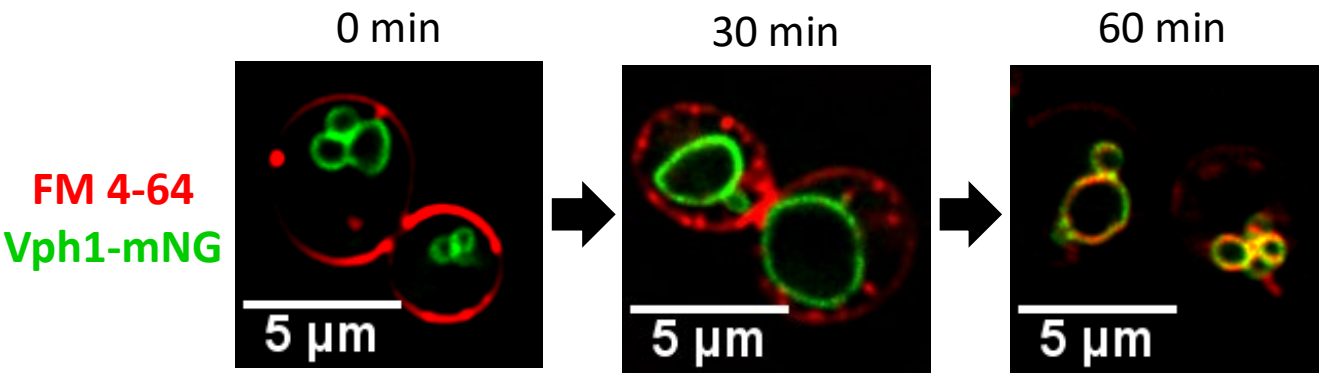

Suppl. Fig. 3B

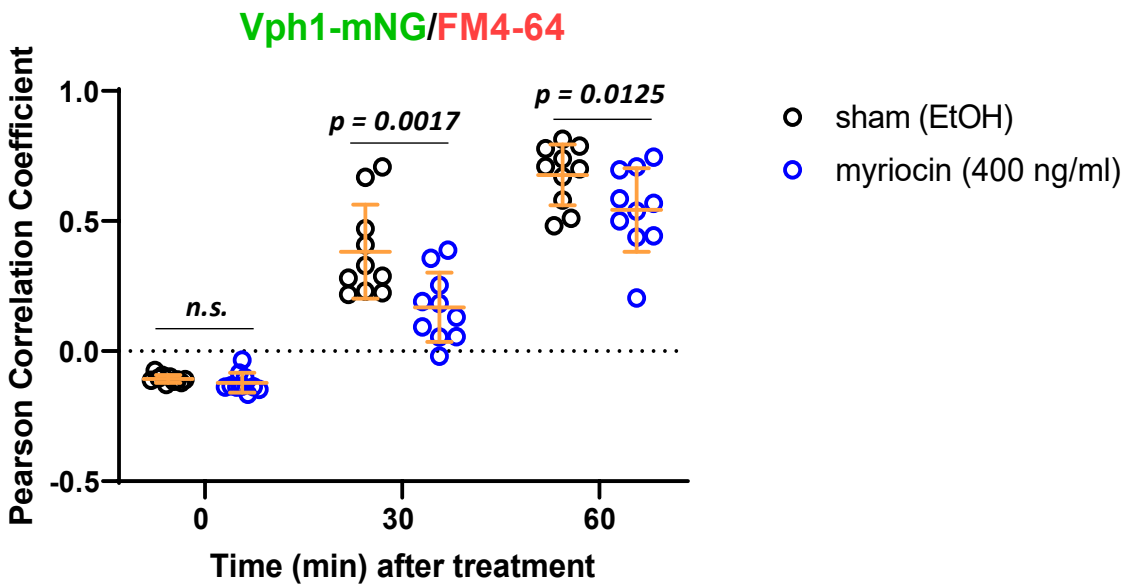

Suppl. Fig. 3C

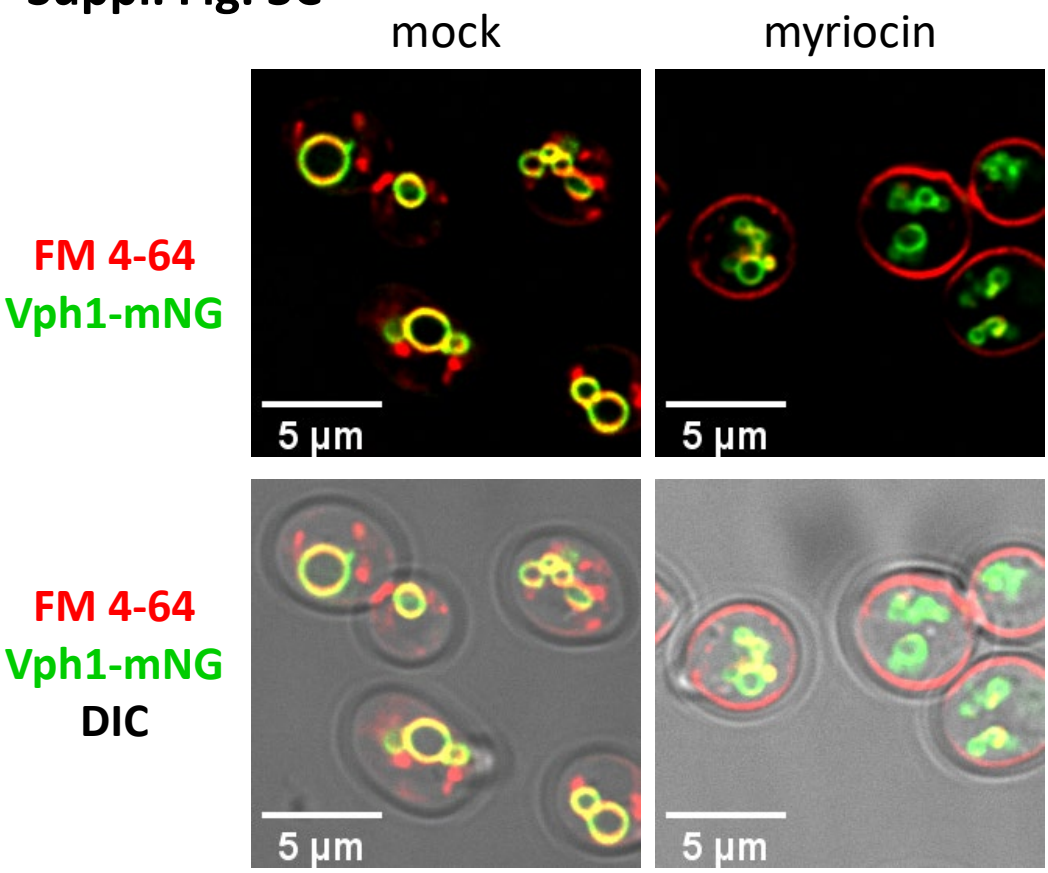

Suppl. Fig. 3D

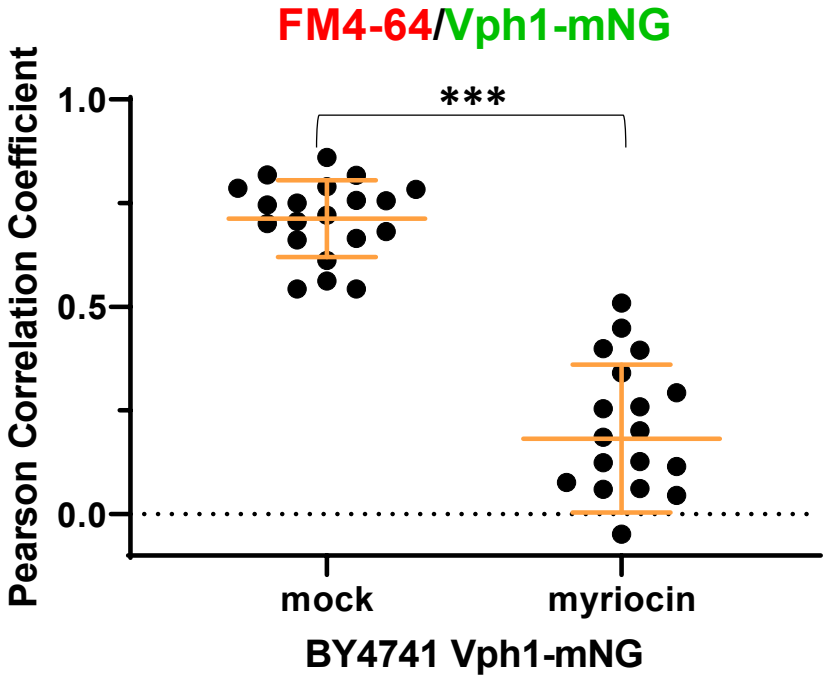

Suppl. Fig. 4A

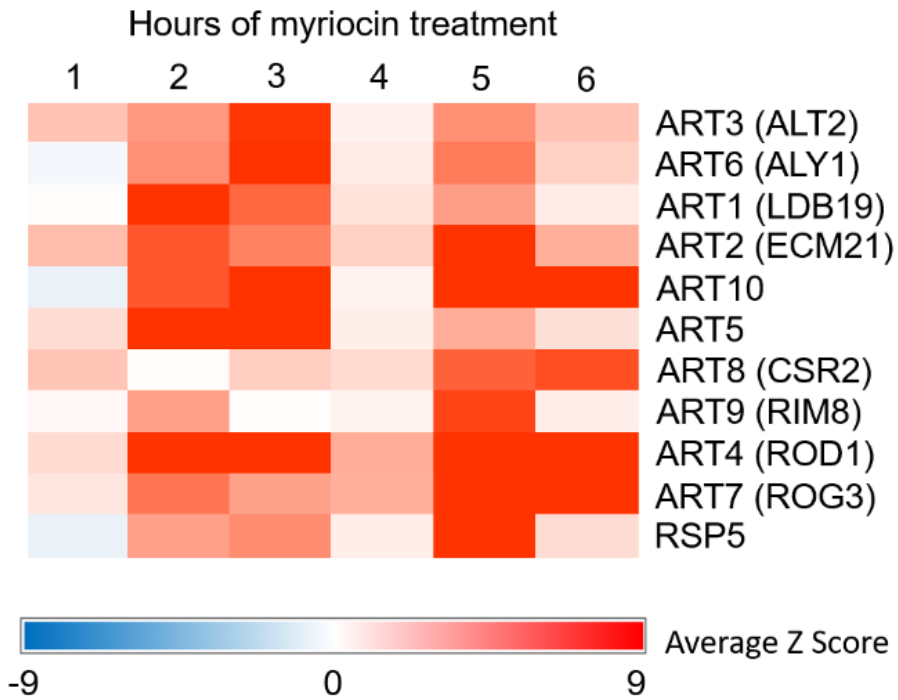

Suppl. Fig. 4B

ART1

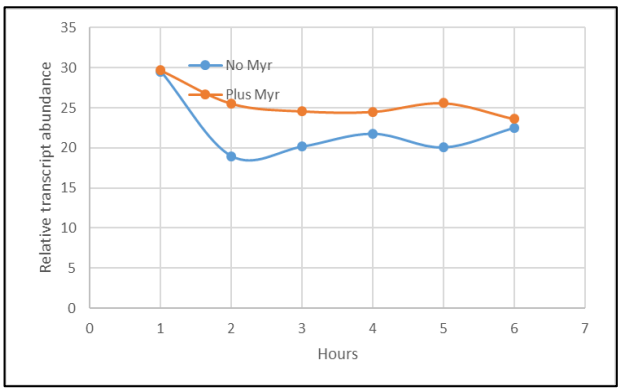

Suppl. Fig. 4C

ART2

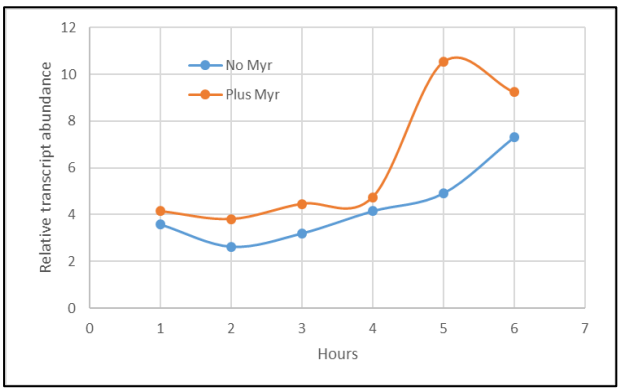

Suppl. Fig. 4D

ART4

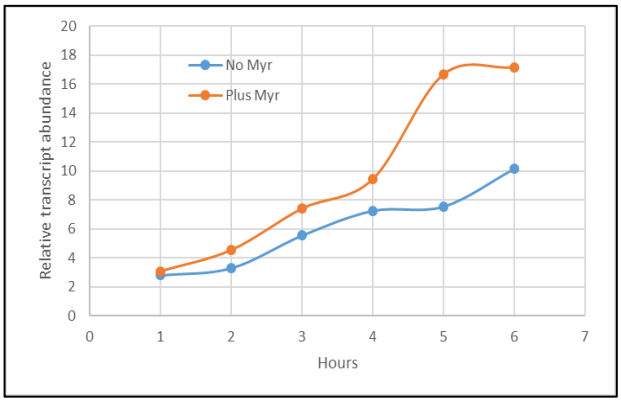

Suppl. Fig. 4E

ART7

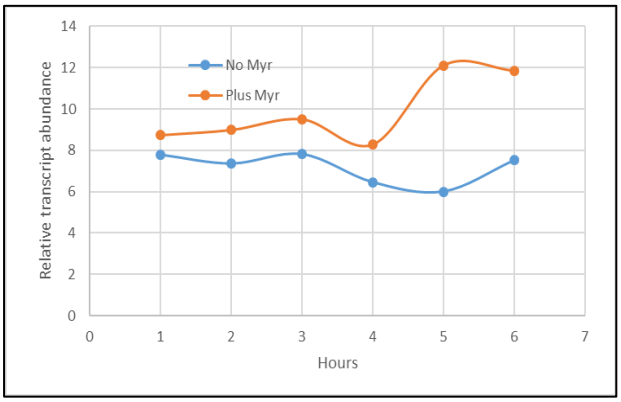

Suppl. Fig. 4F

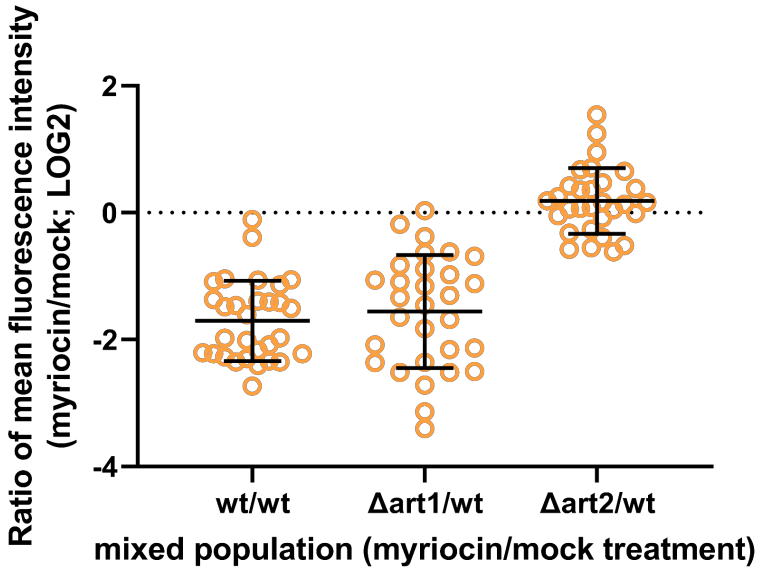

Suppl. Fig. 4G

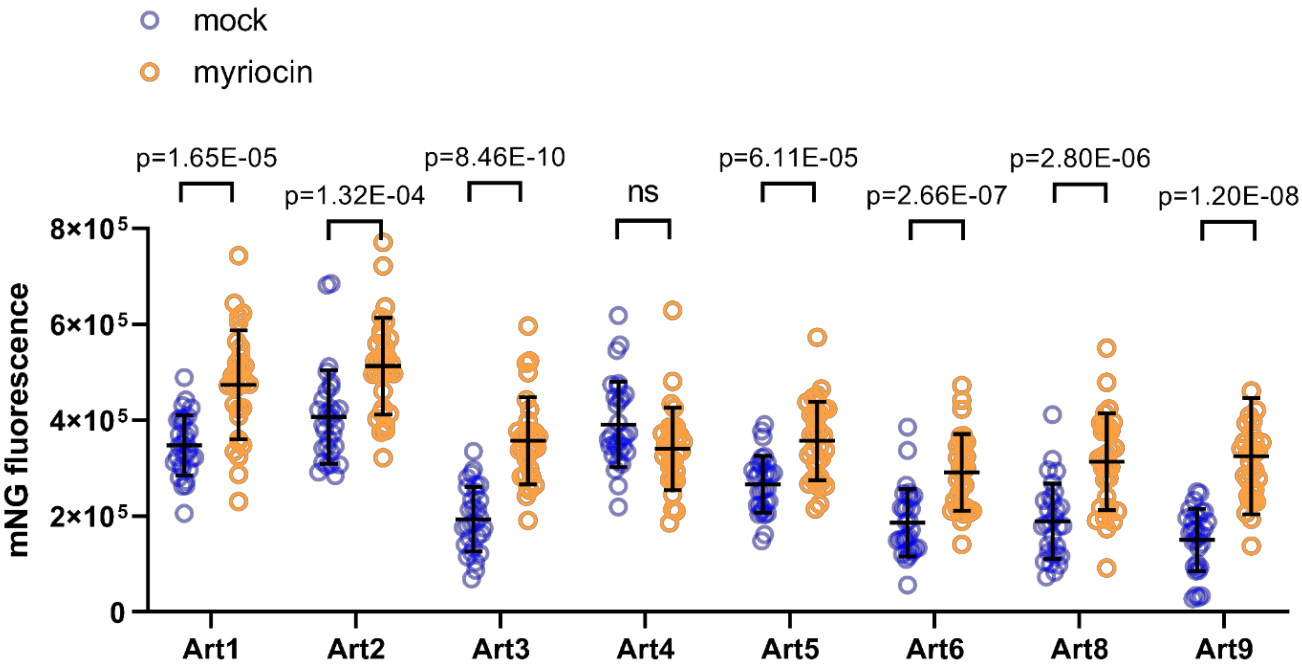

Suppl. Fig. 5

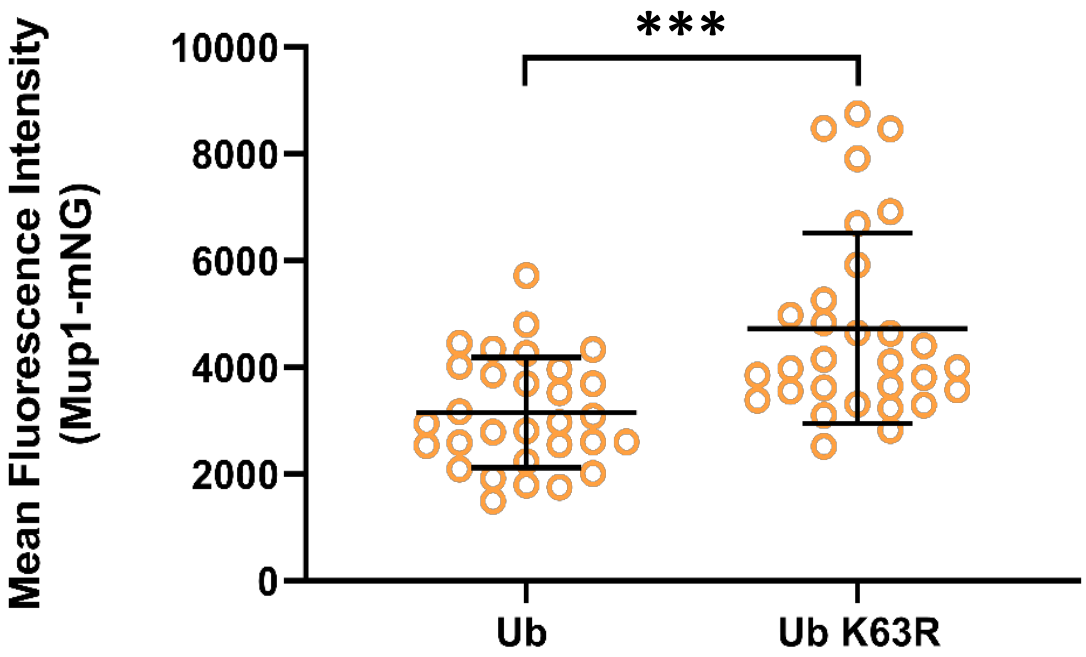
***
Mean Fluorescence Intensity
(Mup1-mNG)
10000
8000
6000
4000
2000
0
Ub
Ub K63R

Suppl. Fig. 6A

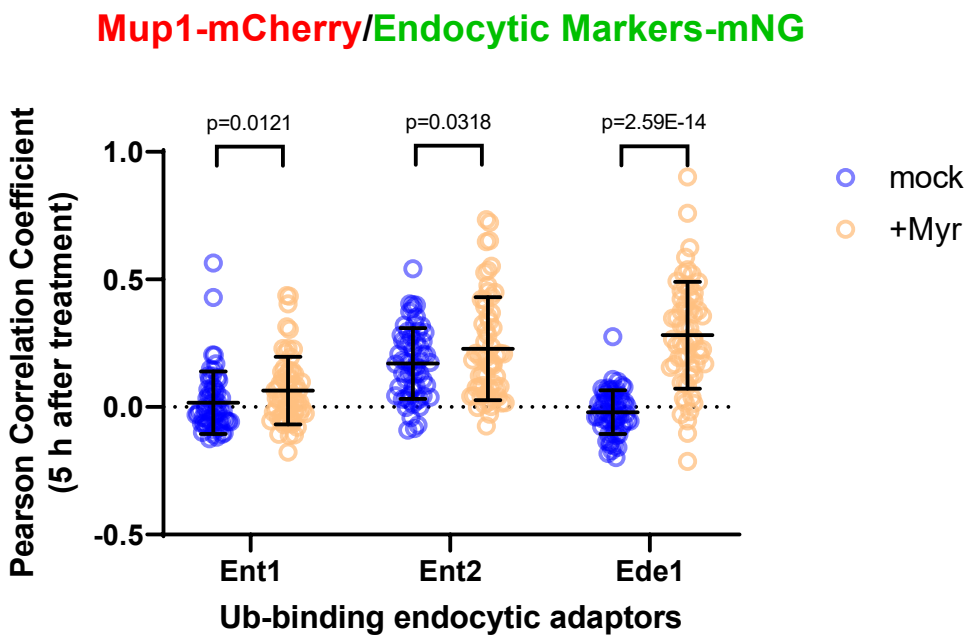

Suppl. Fig. 6B

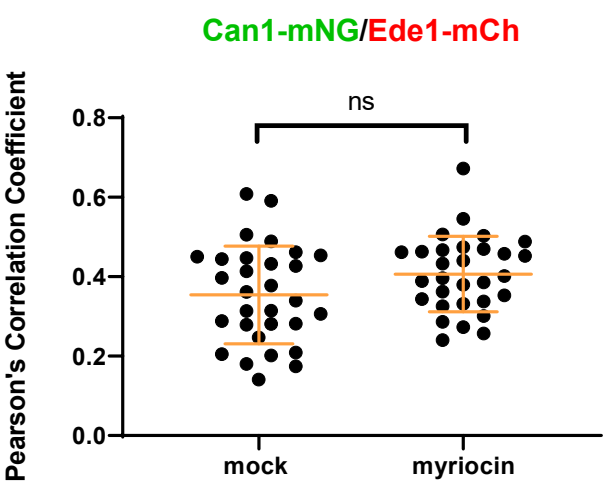

Suppl. Fig. 6C

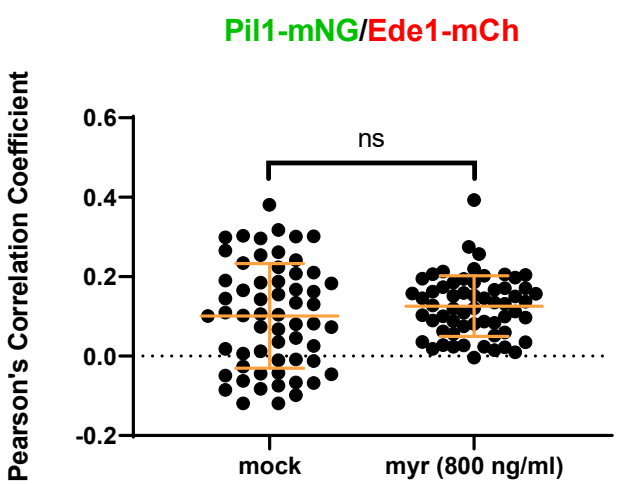

Suppl. Fig. 6D

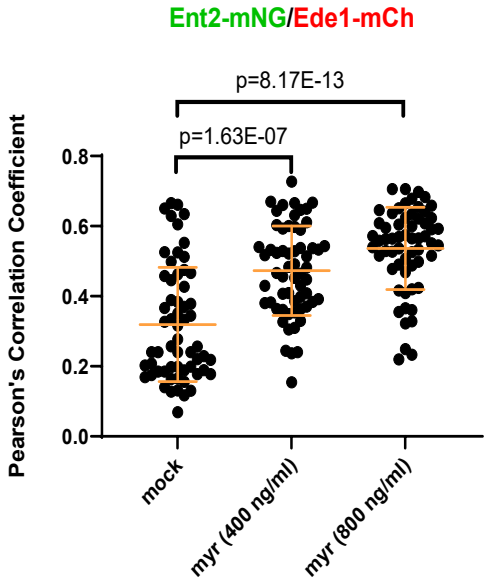

Suppl. Fig. 6E

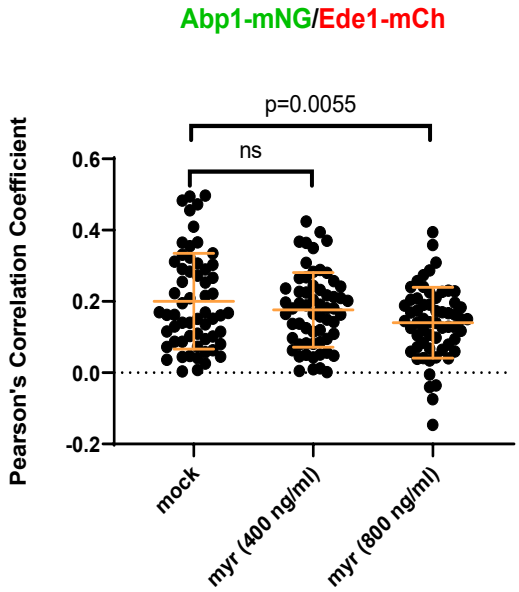

Suppl. Fig. 6F

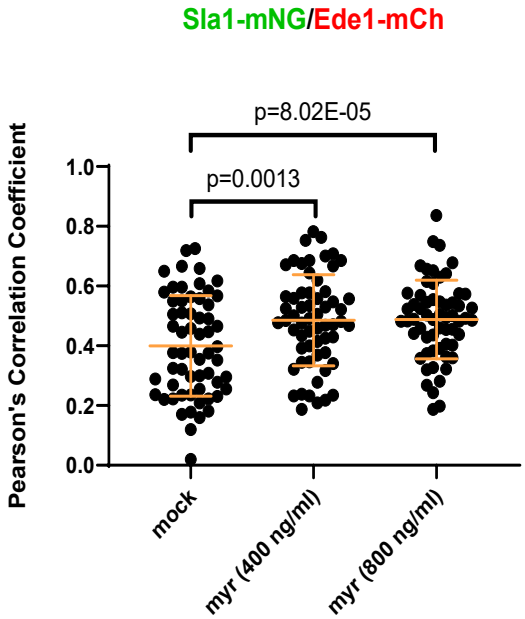

Tables

Table 1. Nutrient transporters and other PM proteins of yeast in response to myriocin treatment.

Functional Classification	PM Protein	Description	Response to Myriocin
amino acid transporters	Mup1	high-affinity Met permease	endocytosis and vacuolar degradation
	Can1	uptake of Arg	no change
	Dip5	uptake of Asp, Glu, Gln, Asn, Ser, Gly and Ala	no change
	Lyp1	uptake of Lys	no change
	Bap3	uptake of Cys, Leu, Ile and Val	increased level at PM
	Tat2	uptake of Trp and Tyr	increased level at PM
	Bap2	high-affinity Leu permease	increased level at PM
	Gnp1	broad specificity amino acid permease	no change
	Hip1	high-affinity His permease	no change
	Gap1	general amino acid permease	no change
hexose transporters	Hxt1	low-affinity glucose transporter	increased level at PM
	Hxt2	high-affinity glucose transporter	increased level at PM
	Hxt3	low-affinity glucose transporter	no change
	Hxt6	high-affinity glucose transporter	no change
proton pumps	Pma1	pumps protons out of cell	no change
	Pma2	pumps protons out of cell	no change
early endocytic proteins	Ent1	epsin protein that binds K63-linked polyUb	increased total level
	Ent2	epsin-like protein that binds K48- or K63-linked polyUb	increased total level
	Ede1	epsin protein that binds K63-linked polyUb	increased total level
	Sla1	cytoskeletal protein binding protein	no change
	Abp1	actin-binding protein	increased total level
	Chc1	clathrin heavy chain	no change
other PM proteins	Ste2	receptor for alpha-factor pheromone	increased level at PM
	Wsc1	sensor-transducer of the stress-activated PKC1-MPK1 kinase pathway	no change
	Pdr5	multidrug and steroid transport	increased level at PM